

# Distortion-resistant and locking-free eight-node elements effectively capturing the edge effects of Mindlin–Reissner plates

Received 25 April 2016  
Revised 13 August 2016  
Accepted 21 August 2016

Yi Bao

*Department of Engineering Mechanics, Tsinghua University, Beijing, China*

Song Cen

*Department of Engineering Mechanics, Tsinghua University, Beijing, China and High Performance Computing Center, Tsinghua University, Beijing, China and Key Laboratory of Applied Mechanics, Tsinghua University, Beijing, China, and*

Chenfeng Li

*Zienkiewicz Centre for Computational Engineering,  
Energy Safety Research Institute, Swansea University, Swansea, UK*

## Abstract

**Purpose** – A simple shape-free high-order hybrid displacement function element method is presented for precise bending analyses of Mindlin–Reissner plates. Three distortion-resistant and locking-free eight-node plate elements are proposed by utilizing this method.

**Design/methodology/approach** – This method is based on the principle of minimum complementary energy, in which the trial functions for resultant fields are derived from two displacement functions,  $F$  and  $f$ , and satisfy all governing equations. Meanwhile, the element boundary displacements are determined by the locking-free arbitrary order Timoshenko's beam functions. Then, three locking-free eight-node, 24-DOF quadrilateral plate-bending elements are formulated: HDF-P8-23 $\beta$  for general cases, HDF-P8-SS1 for edge effects along soft simply supported (SS1) boundary and HDF-P8-FREE for edge effects along free boundary.

**Findings** – The proposed elements can pass all patch tests, exhibit excellent convergence and possess superior precision when compared to all other existing eight-node models, and can still provide good and stable results even when extremely coarse and distorted meshes are used. They can also effectively solve the edge effect by accurately capturing the peak value and the dramatical variations of resultants near the SS1 and free boundaries. The proposed eight-node models possess potential in engineering applications and can be easily integrated into commercial software.

**Originality/value** – This work presents a new scheme, which can take the advantages of both analytical and discrete methods, to develop high-order mesh distortion-resistant Mindlin–Reissner plate-bending elements.

**Keywords** Plate bending, Finite element methods, Analytical trial function, Edge effect, Hybrid displacement function element

**Paper type** Research paper



## 1. Introduction

The availability of simple, efficient and reliable elements for thin and thick plates represents one of the main features of all finite element computer program libraries for structural analysis. To date, considerable research efforts have been made to develop various plate-bending elements (Bathe, 1996; Cen and Shang, 2015; Long *et al.*, 2009; Zienkiewicz and Taylor, 2000), in which many models are based on the Mindlin–Reissner plate theory (Mindlin, 1951; Reissner, 1945). Unlike the thin-plate theory which requires  $C_1$  continuity between the displacement fields of two adjacent elements, Mindlin–Reissner plate theory only requires  $C_0$  continuity and can be used for both thin and moderately thick plates (Crisfield, 1984).

Most conventional Mindlin–Reissner plate elements are displacement-based models and generally perform well in moderately thick-plate applications. However, when the span-to-thickness ratio of the plate becomes very large, their performances often become over-stiff, so they are not reliable for thin-plate cases. This numerical difficulty is known as the transverse shear locking caused by false shear strains. During the history of finite element method, many investigators proposed recognized treatments on shear locking, including the classical reduced (Zienkiewicz *et al.*, 1971) and selective reduced integral schemes (Hughes *et al.*, 1977), the stabilization procedure for reduced integral (Belytschko *et al.*, 1981; Belytschko and Tsay, 1983), the mixed interpolated tensorial components techniques (Bathe and Dvorkin 1985, 1986), the substitute shear–strain methods (Hinton and Huang, 1986; Onate *et al.*, 1992), the mixed-element method derived from the modified Hellinger–Reissner principle (Lee and Wong, 1982), the linked interpolation schemes (Taylor and Auricchio, 1993; Zienkiewicz *et al.*, 1993), the discrete shear constraint methods (Batoz and Lardeur, 1989; Katili, 1993), the hybrid-mixed variational approach (Ayad *et al.*, 1998; Ayad and Rigolot, 2002), the enhanced displacement interpolation (Ibrahimbegović, 1993), the improved interpolation based on locking-free Timoshenko's beam formulae (Chen and Cheung, 2000; Soh *et al.*, 1999a, 1999b, 2001), the generalized conforming Mindlin–Reissner plate element (Cen *et al.*, 2006) based on the quadrilateral area coordinates (Long *et al.*, 1999a; Long *et al.*, 1999b; Long *et al.*, 2009), the smoothed FEM(SFEM) (Nguyen-Thoi *et al.*, 2012; Nguyen-Xuan *et al.*, 2008, 2009), etc. (Cen *et al.*, 2002; Falsone and Settineri, 2012; Hansbo *et al.*, 2011; Hu *et al.*, 2010; Jin *et al.*, 1993; Jin and Qin, 1995; Jirousek *et al.*, 1995a, 1995b; Nguyen-Thanh *et al.*, 2011; Petrolito, 1990, 1996; Rezaiee-Pajand and Karkon, 2012; Ribaric and Jelenic, 2012). On the other hand, high-order elements usually have better precisions and exhibit better performance for thin-plate cases. So, many attempts have also been devoted to construct high-order models free of shear locking. Ahmad *et al.* (1970) applied the Mindlin–Reissner plate theory in the degenerated shell approach and developed an eight-node isoparametric element; Crisfield (1984) developed a quadratic element using shear constraints; Spilker and Munir (1980) and Spilker (1982) proposed eight-node hybrid-stress elements for analysis of thin and moderately thick plates; Hughes and Cohen (1978) presented a so-called “heterosis” element which used an eight-node interpolation for rotations and nine-node interpolations for deflections; Kant *et al.* (1982) proposed an element based on a higher-order displacement mode and a three-dimensional state of stress and strain; Hinton and Huang (1986) developed a family of elements, including 8-, 9-, 12- and 16-node elements, with substitute strain fields; Donea and Lamain (1987) provided a modified representation of transverse shear component in eight- and nine-node quadrilateral plate elements; Polit *et al.* (1994) proposed an eight-node quadrilateral element, in which each monomial term of the interpolation functions for the normal rotations is matched by the derivatives of its corresponding deflection; Zhang and Kuang (2007) developed a new eight-node Reissner–Mindlin plate element with a special interpolation within the element, and

this special interpolation is an extension of the element boundary interpolation that uses Timoshenko beam function for the boundary segment interpolation; Dhananjaya *et al.* (2009) adopted the integrated force method to construct an eight-node serendipity quadrilateral thin-thick plate-bending element (MQP8); Li *et al.* (2015) presented an eight-node quadrilateral assumed stress hybrid Mindlin plate element with 39 unknown parameters. These efforts more or less improved the element resistance to shear locking problem.

In addition to the above shear locking problem, how to obtain good resultant/stress solutions is another problem that should need attention. For a Mindlin–Reissner plate, its rotations and stress resultants may vary sharply in a narrow region in the vicinity of certain types of boundary conditions. This is the so-called edge effect or the boundary layer effect, and it represents another interesting and troublesome numerical challenge in the Mindlin–Reissner plate theory (Arnold and Falk, 1989). However, the aforementioned efforts mainly concentrate on the shear-locking problem, and few solution strategies have been considered for solving this difficulty. Although the edge effect does not impose great influences on the entire structure, it will complicate the numerical analysis. Some analytical, semi-analytical and discrete methods have been proposed to conquer this challenging topic (Arnold and Falk, 1990; Babusôka and Scapolla, 1989; Briassoulis, 1993a, 1993b; Hagglad and Bathe, 1990; Hinton *et al.*, 1995; Kant and Gadgil, 2002; Kant and Hinton, 1983; Rao *et al.*, 1992; Schwab and Suri, 1996; Wang *et al.*, 2002; Ye and Yuan, 2002; Yuan, 1993; Yuan *et al.*, 1998), but few finite element models can easily and accurately predict the distributions of the resultants near the plate boundaries when edge effect takes place.

Besides good behaviors in dealing with shear locking and edge effect problems, an ideal plate-bending element should have following features:

- no adjusted factor existing in its formulations;
- high tolerance to various mesh distortions; and
- high-precision results for stress/resultant solutions and displacements.

Recently, to develop plane quadrilateral elements immune to mesh distortions, Fu *et al.* (2010) and Cen *et al.* (2011a, 2011b, 2011c) proposed a simple hybrid stress function (HSF) element method, in which the trial functions for stress fields are the analytical solutions of the stress function  $\phi$ . Inheriting from this technique, Cen *et al.* (2014) and Shang *et al.* (2015) established a simple hybrid displacement function (HDF) element method for constructing Mindlin–Reissner plate bending elements, in which the trial functions for resultant fields are derived from two displacement functions,  $F$  and  $f$  (Hu, 1984), and satisfy all governing equations. Then, a robust shape-free four-node, 12-DOF quadrilateral element HDF-P4-11 $\beta$  for general cases, two shape-free four-node, 12-DOF quadrilateral elements HDF-P4-Free and HDF-P4-SS1 for solving edge effects along free and soft simply supported (SS1) boundaries, respectively, were successfully developed. Numerical examples proved that these new models possess outstanding performances among all existing four-node models, no matter for conventional problems, or for edge effects.

Actually, the aforementioned hybrid displacement function element method can be simply extended to construct higher-order elements, so that more precise results for both displacements and resultants, especially for the resultant distributions with edge effects, can be obtained using fewer elements. In this paper, three different eight-node, 24-DOF quadrilateral Mindlin–Reissner plate-bending elements for different purpose are presented. For general situation, 23 sets of the resultant components derived from the displacement function  $F$  and satisfying all governing equations are taken as the trial functions for resultant fields. Meanwhile, the element boundary displacements and shear strains are determined by

the locking-free arbitrary order Timoshenko's beam functions (Jelenic and Papa, 2011). Then, an eight-node, 24-DOF quadrilateral plate-bending element, HDF-P8-23 $\beta$ , is first formulated by the principle of minimum complementary energy. For special situations consisting of the edge effect or the boundary layer effect (SS1 and FREE types), the additional displacement function  $f$  related to the edge effect is considered. Then, two new eight-node, 24-DOF quadrilateral elements, denoted by HDF-P8-SS1 and HDF-P8-FREE, are also constructed. The proposed elements pass all the patch tests, exhibit excellent convergence and possess superior precision when compared to other existing eight-node models, and can still provide good and stable results even when extremely coarse and distorted meshes are used. It can also effectively solve the edge effect by accurately capturing the peak value and the dramatical variations of resultants near the SS1 and free boundaries. The proposed eight-node models possess the potential in the engineering application and could be easily integrated into the commercial software.

## 2. The arbitrary order Timoshenko's beam functions

For a robust Mindlin–Reissner plate-bending element, it is necessary to eliminate the phenomenon of shear locking which induces an over-stiff problem as the plate becomes progressively thinner. So, how to determine whether rational displacement modes and shear strains along element edges become a key technique for many existing models. In the formulations of some low-order plate elements, a set of locking-free functions for two-node Timoshenko beam have been successfully applied (Cen *et al.*, 2002, 2006, 2014; Chen and Cheung, 2000; Soh *et al.*, 1999a, 1999b, 2001; Shang *et al.*, 2015). Recently, Jelenic and Papa (2011) presented a set of new arbitrary-order Timoshenko beam functions. These functions are given by:

$$w = \sum_{i=1}^n I_i w_i - \frac{L}{n} \prod_{j=1}^n N_j \sum_{i=1}^n (-1)^{i-1} \binom{n-1}{i-1} \psi_i, \quad \psi = \sum_{i=1}^n I_i \psi_i \quad (1)$$

where  $L$  is the beam length;  $w_i$  and  $\psi_i$  ( $i = 1 \sim n$ ) are the nodal displacements and the rotations at the  $n$ th nodes equidistantly located between the beam ends;  $I_i$  ( $i = 1 \sim n$ ) are the standard Lagrange polynomials of order  $n - 1$ :

$$\begin{cases} \text{for } j = 1, & N_j = \frac{r}{L} \\ \text{else, } N_j = 1 - \frac{(n-1)r}{(j-1)L} \end{cases} \quad (2)$$

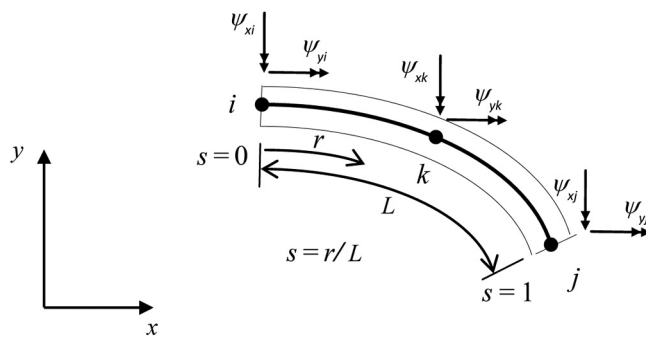
in which,  $r$  is the length along the beam from the starting point. For an eight-node quadrilateral element, any quadrilateral side can be treated as a three-node Timoshenko beam element as given in Figure 1. Then, the displacement and rotations can be obtained:

$$\bar{w} = I_a w_i + I_b w_j + I_c w_k - I_0 [(\psi_{xi} + \psi_{xj} - 2\psi_{xk}) l_x^* - (\psi_{yi} + \psi_{yj} - 2\psi_{yk}) l_y^*] \quad (3)$$

$$\bar{\psi}_x = I_a \psi_{xi} + I_b \psi_{xj} + I_c \psi_{xk}, \quad \bar{\psi}_y = I_a \psi_{yi} + I_b \psi_{yj} + I_c \psi_{yk} \quad (4)$$

With:

**Figure 1.**  
Timoshenko's beam element (curved)



$$\begin{cases} L_1 = 1 - s, L_2 = s, I_a = L_1(2L_1 - 1), I_b = L_2(2L_2 - 1), I_c = 4L_1L_2, I_0 = \frac{L_1L_2(L_2 - L_1)}{3} \\ l_x^* = (4s - 3)x_i + (4s - 1)x_j + (4 - 8s)x_k, l_y^* = -(4s - 3)y_i - (4s - 1)y_j - (4 - 8s)y_k \\ l_x = \frac{-l_y^*}{(l_x^{*2} + l_y^{*2})^{\frac{1}{2}}}, l_y = \frac{-l_x^*}{(l_x^{*2} + l_y^{*2})^{\frac{1}{2}}} \end{cases} \quad (5)$$

in which  $s = r/L$  is the local coordinate along the beam (varies from 0 to 1). One should notice here that the formulations are valid for curved boundaries because, at different points along the boundaries, different tangent directions and outer normal directions could be derived by applying a differential method.

Thus, the displacement components  $\bar{\mathbf{u}}$  along the  $i-j-k$  boundary can be written as:

$$\bar{\mathbf{u}}_{ijk} = \begin{Bmatrix} \bar{w} \\ \psi_x \\ \psi_y \end{Bmatrix} = \begin{bmatrix} I_a & -I_0l_x^* & I_0l_y^* & I_b & -I_0l_x^* & I_0l_y^* & I_c & 2I_0l_x^* & -2I_0l_y^* \\ 0 & I_a & 0 & 0 & I_b & 0 & 0 & I_c & 0 \\ 0 & 0 & I_a & 0 & 0 & I_b & 0 & 0 & I_c \end{bmatrix} \mathbf{q}_{ijk} = \mathbf{L}_{abc} \mathbf{q}_{ijk} \quad (6)$$

where:

$$\mathbf{q}_{ijk} = [\mathbf{q}_i \quad \mathbf{q}_j \quad \mathbf{q}_k]^T, \mathbf{q}_m = [w_m \quad \psi_{xm} \quad \psi_{ym}]^T (m = i, j, k) \quad (7)$$

### 3. The general formulations of the HDF elements

At the element level, the finite element equations can be written as:

$$\mathbf{K}^e \mathbf{q}^e = \mathbf{P}_q^e \quad (8)$$

in which  $\mathbf{K}^e$  is the element stiffness matrix;  $\mathbf{q}^e$  is the element nodal displacement vector; and  $\mathbf{P}_q^e$  is the element nodal equivalent load vector caused by the distributed transverse load  $\mathbf{q}$ .

Following the construction procedure of the hybrid-displacement function elements (Cen *et al.*, 2014), the element stiffness matrix of the Mindlin–Reissner plates can be obtained:

---


$$\mathbf{K}^e = \mathbf{H}^T \mathbf{M}^{-1} \mathbf{H} \quad (9) \quad \text{Eight-node elements}$$

$$\mathbf{P}_q^e = \mathbf{V}^T - \mathbf{H}^T \mathbf{M}^{-1} \mathbf{M}^* \quad (10)$$

where:

$$\mathbf{M} = \iint_{A^e} \hat{\mathbf{S}}^T \mathbf{C} \hat{\mathbf{S}} dx dy, \quad \mathbf{M}^* = \iint_{A^e} \hat{\mathbf{S}}^T \mathbf{C} \mathbf{R}^* dx dy, \quad \mathbf{Q} = \iint_{A^e} \mathbf{R}^{*T} \mathbf{C} \mathbf{R}^* dx dy \quad (11) \quad \text{553}$$

$$\mathbf{H} = \int_{S^e} \hat{\mathbf{S}}^T \mathbf{L}^T \bar{\mathbf{N}}|_{\Gamma} ds, \quad \mathbf{V} = \int_{S^e} \mathbf{R}^{*T} \mathbf{L}^T \bar{\mathbf{N}}|_{\Gamma} ds \quad (12)$$

In above equations,  $\hat{\mathbf{S}}$  represents the general solution part;  $\mathbf{R}^*$  represents the corresponding particular solutions of the resultant forces (for different distributions of the transverse load  $q$ ,  $\mathbf{R}^*$  is also different); and  $\mathbf{C}$  is the flexibility matrix:

$$\mathbf{C} = \begin{bmatrix} \frac{1}{D(1-\mu^2)} & \frac{-\mu}{D(1-\mu^2)} & 0 & 0 & 0 \\ \frac{-\mu}{D(1-\mu^2)} & \frac{1}{D(1-\mu^2)} & 0 & 0 & 0 \\ 0 & 0 & \frac{2}{D(1-\mu)} & 0 & 0 \\ 0 & 0 & 0 & \frac{1}{C} & 0 \\ 0 & 0 & 0 & 0 & \frac{1}{C} \end{bmatrix} \quad (13)$$

with  $\mu$  denoting Poisson's ratio and  $D$  the bending stiffness of the plate;  $\mathbf{L}$  denotes the matrix of the direction cosines for element boundaries:

$$\mathbf{L} = \begin{bmatrix} l_x^2 & l_y^2 & 2l_x l_y & 0 & 0 \\ -l_x l_y & l_x l_y & l_x^2 - l_y^2 & 0 & 0 \\ 0 & 0 & 0 & -l_x & -l_y \end{bmatrix} \quad (14)$$

where  $l_x$  and  $l_y$  denote the direction cosines of outer normal of the element boundary;  $\bar{\mathbf{N}}|_{\Gamma}$  is the interpolation matrix for boundary displacements, and it has different values along each element edge. The components of  $\bar{\mathbf{N}}|_{\Gamma}$  are derived from the formulae of the arbitrary-order Timoshenko's beam functions given in the last section ([Jelenic and Papa, 2011](#)), and their detailed expressions are given in the [Appendix](#).

According to [Hu \(1984\)](#), the solutions of rotations  $\psi_x$ ,  $\psi_y$  and deflection  $w$  for a Mindlin–Reissner plate can be expressed by:

$$\psi_x = \frac{\partial F}{\partial x} + \frac{\partial f}{\partial y}, \quad \psi_y = \frac{\partial F}{\partial y} - \frac{\partial f}{\partial x}, \quad w = F - \frac{D}{C} \nabla^2 F \quad (15)$$

with:

$$D = \frac{Eh^3}{12(1 - \mu^2)}, \quad C = \frac{5}{6}Gh \quad (16)$$

where  $h$  is the plate thickness;  $E$  is the Young's modulus;  $G = E/[2(1 + \mu)]$  is the shear modulus;  $F$  and  $f$  in [equation \(15\)](#) are two displacement functions and satisfy the following equations

554

$$D\nabla^2\nabla^2F = q \quad (17)$$

$$\frac{1}{2}(1 - \mu)D\nabla^2f - Cf = 0 \quad (18)$$

in which,  $q$  is the distributed transverse load. From [equations \(9\) to \(12\)](#), the key point for formulating the HDF elements is to define the general solution part  $\bar{\mathbf{S}}$  and the corresponding particular solutions  $\mathbf{R}^*$  of the resultant forces which can be derived from the two displacement functions  $F$  and  $f$ .

### 3.1 Formulations of element HDF-P8-23P (without edge effects)

[Figure 2](#) shows an eight-node quadrilateral plate-bending element. In normal situations, the first displacement function  $F$  in [equation \(17\)](#) is capable of reflecting the deformation of a Mindlin–Reissner plate. Based on the derivations given by [Cen et al. \(2014\)](#), the trial

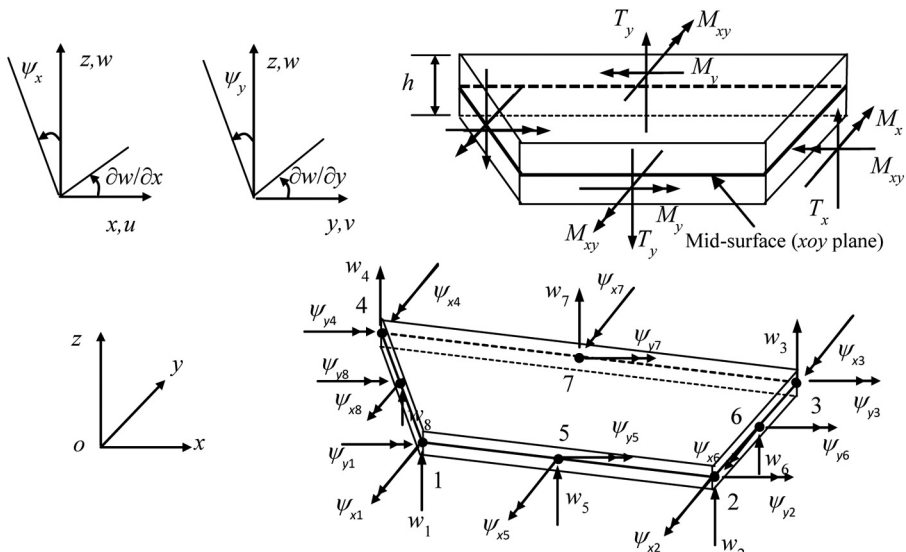


**Figure 2.**  
Shape-free eight-node quadrilateral plate bending element

functions for the resultant forces without edge effects can be expressed by the displacement function  $F$  as:

Eight-node elements

$$\mathbf{R}_{\text{normal}} = \begin{Bmatrix} M_x \\ M_y \\ M_{xy} \\ T_x \\ T_y \end{Bmatrix} = \mathbf{R}^0 + \mathbf{R}^* = \sum_{i=1}^k \mathbf{R}_i^0 \beta_i + \mathbf{R}^* = \hat{\mathbf{S}} \boldsymbol{\beta} + \mathbf{R}^* \quad (19) \quad \underline{\underline{555}}$$

with:

$$\mathbf{R}^0 = \sum_{i=1}^k \mathbf{R}_i^0 \beta_i, \quad \mathbf{R}^0 = \begin{Bmatrix} M_x^0 \\ M_y^0 \\ M_{xy}^0 \\ T_x^0 \\ T_y^0 \end{Bmatrix} = \begin{Bmatrix} \frac{\partial^2 F^0}{\partial x^2} + \mu \frac{\partial^2 F^0}{\partial y^2} \\ \frac{\partial^2 F^0}{\partial y^2} + \mu \frac{\partial^2 F^0}{\partial x^2} \\ (1 - \mu) \frac{\partial^2 F^0}{\partial x \partial y} \\ \frac{\partial}{\partial x} (\nabla^2 F^0) \\ \frac{\partial}{\partial y} (\nabla^2 F^0) \end{Bmatrix}, \quad \mathbf{R}^* = \begin{Bmatrix} M_x^* \\ M_y^* \\ M_{xy}^* \\ T_x^* \\ T_y^* \end{Bmatrix}$$

$$= \begin{Bmatrix} -\frac{q}{4}(x^2 + \mu y^2) \\ -\frac{q}{4}(\mu x^2 + y^2) \\ 0 \\ -\frac{q}{2}x \\ -\frac{q}{2}y \end{Bmatrix} \quad (20)$$

$$\hat{\mathbf{S}} = \left[ \mathbf{R}_1^0 \quad \mathbf{R}_2^0 \quad \dots \quad \mathbf{R}_k^0 \right]_{5 \times k} \quad (21)$$

where  $\beta^*$  ( $I = 1 \sim k$ ) are  $k$  unknown coefficients;  $F_i^0$  are the ( $I = 1 \sim k$ )  $k$  analytical solutions (in Cartesian coordinates) of  $F^0$  which are generated from the homogeneous equation of [equation \(17\)](#). The first 23 analytical solutions of  $F^0$  (seventh-order completed in Cartesian coordinates) and related resultant solutions are given in [Table I](#). Meanwhile,  $\mathbf{R}^*$  represents the corresponding particular solutions of the resultant forces under uniformly distributed transverse load  $q$  (for transverse load  $q$  with different distributions,  $\mathbf{R}^*$  is also different).

After substituting the corresponding  $\hat{\mathbf{S}}$  and  $\mathbf{R}^*$  into [equations \(9\) to \(12\)](#), a new eight-node quadrilateral plate-bending element is constructed. This element is denoted by HDF-P8-23 $\beta$  (without edge effects), and it is very easy to be integrated into the standard framework of finite element programs.

$i$	1	2	3	4	5	6	7
$-DF_i^0$	$x^2$	$xy$	$y^2$	$x^3$	$x^2y$	$xy^2$	$y^3$
$M_x^0$	2	0	$2\mu$	$6x$	$2y$	$2\mu x$	$6\mu y$
$M_y^0$	$2\mu$	0	2	$6\mu x$	$2\mu y$	$2x$	$6y$
$M_{xy}^0$	0	$1-\mu$	0	0	$2(1-\mu)x$	$2(1-\mu)y$	0
$T_x^0$	0	0	0	6	0	2	0
$T_y^0$	0	0	0	0	2	0	6
$i$	8		9		10		11
$-DF_i^0$	$x^3y$		$xy^3$		$x^4-y^4$		$6x^2y^2-x^4-y^4$
$M_x^0$	$6xy$		$6\mu xy$		$12(x^2-\mu y^2)$		$12(1-\mu)(y^2-x^2)$
$M_y^0$	$6\mu xy$		$6xy$		$-12(y^2-\mu x^2)$		$12(1-\mu)(x^2-y^2)$
$M_{xy}^0$	$3(1-\mu)x^2$		$3(1-\mu)y^2$		0		$24(1-\mu)xy$
$T_x^0$	6y		6y		24x		0
$T_y^0$	6x		6x		-24y		0
$i$	12		13		14		
$-DF_i^0$	$x^3y^2-xy^4$		$5x^3y^2-x^5$		$x^2y^3-x^4y$		
$M_x^0$	$6xy^2+\mu(2x^3-12xy^2)$		$10\mu x^3-20x^3+30xy^2$		$6\mu x^2y+2y^3-12x^2y$		
$M_y^0$	$6\mu xy^2+2x^3-12xy^2$		$10x^3+\mu(-20x^3+30xy^2)$		$6x^2y+\mu(2y^3-12x^2y)$		
$M_{xy}^0$	$(1-\mu)(6x^2y-4y^3)$		$30(1-\mu)x^2y$		$(1-\mu)(6xy^2-4x^3)$		
$T_x^0$	$6(x^2-y^2)$		$-30x^2+30y^2$		-12xy		
$T_y^0$	-12xy		60xy		$6(-x^2+y^2)$		
$i$	15		16		17		
$-DF_i^0$	$5x^2y^3-y^5$		$x^5y-xy^5$		$10x^3y^3-3x^5y-3xy^5$		
$M_x^0$	$10y^3+\mu(-20y^3+30x^2y)$		$-20\mu xy^3+20x^3y$		$60(1-\mu)(xy^3-x^3y)$		
$M_y^0$	$10\mu y^3-20y^3+30x^2y$		$-20xy^3+20\mu x^3y$		$60(1-\mu)(x^3y-xy^3)$		
$M_{xy}^0$	$30(1-\mu)xy^2$		$5(1-\mu)(x^4-y^4)$		$-15(1-\mu)(x^4-6x^2y^2+y^4)$		
$T_x^0$	60xy		$60x^2y-20y^3$		0		
$T_y^0$	$30x^2-30y^2$		$20x^3-60xy^2$		0		
$i$	18				19		
$-DF_i^0$	$x^6-10x^4y^2+5x^2y^4$				$y^6-10x^2y^4+5x^4y^2$		
$M_x^0$	$30x^4-120x^2y^2+10y^4+\mu(-20x^4+60x^2y^2)$				$-20y^4+60x^2y^2+\mu(30y^4-120x^2y^2+10x^4)$		
$M_y^0$	$-20x^4+60x^2y^2+\mu(30x^4-120x^2y^2+10y^4)$				$30y^4-120x^2y^2+10x^4+\mu(-20y^4+60x^2y^2)$		
$M_{xy}^0$	$40(1-\mu)(-2x^3y+xy^3)$				$40(1-\mu)(-2xy^3+x^3y)$		
$T_x^0$	$40x^3-120xy^2$				$40x^3-120xy^2$		
$T_y^0$	$40y^3-120x^2y$				$40y^3-120x^2y$		
$i$	20				21		
$-DF_i^0$	$21x^5y^2-2x^7-7xy^6$				$35x^4y^3-y^7-14x^6y$		
$M_x^0$	$42(-2x^5+10x^3y^2)+42\mu(x^5-5xy^4)$				$420(-x^4y+x^2y^3)+42\mu(5x^4y-y^5)$		
$M_y^0$	$42(x^5-5xy^4)+42\mu(-2x^5+10x^3y^2)$				$42(5x^4y-y^5)+420\mu(-x^4y+x^2y^3)$		
$M_{xy}^0$	$42(1-\mu)(5x^4y-y^5)$				$84(1-\mu)(5x^3y^2-x^5)$		
$T_x^0$	$-210(x^4-6x^2y^2+y^4)$				$-840(x^3y-xy^3)$		
$T_y^0$	$840(x^3y-xy^3)$				$-210(x^4-6x^2y^2+y^4)$		
$i$	22				23		
$-DF_i^0$	$35x^3y^4-x^7-14xy^6$				$21x^2y^5-2y^7-7x^6y$		
$M_x^0$	$42(5x^4-y^5)+420\mu(-xy^4+x^3y^2)$				$42(5x^4-y^5)+420\mu(-2y^5+10x^2y^3)$		
$M_y^0$	$420(-xy^4+x^3y^2)+42\mu(5xy^4-x^5)$				$42(-2y^5+10x^2y^3)+42\mu(y^5-5x^4y)$		
$M_{xy}^0$	$84(1-\mu)(5x^2y^3-y^5)$				$42(1-\mu)(5xy^4-x^5)$		
$T_x^0$	$-210(x^4-6x^2y^2+y^4)$				$-840(x^3y-xy^3)$		
$T_y^0$	$840(x^3y-xy^3)$				$-210(x^4-6x^2y^2+y^4)$		

**Table I.**  
 Twenty-three  
 fundamental  
 analytical solutions  
 for the general part  
 of the displacement  
 function and  
 resulting resultant  
 forces

---

3.2 Formulations of elements HDF-P8-SS1 (with SS1 edge effects) and HDF-P8-FREE (with free edge effects)

When the edge effect is taken into consideration, the second displacement function  $f$  has a significant effect on the performance of the elements. In the vicinity of certain types of boundary conditions, it has a significant value near the plate boundaries, but it can be ignored in other areas (Shang *et al.*, 2015).

After considering the second displacement function  $f$ , the resultant forces with edge effects can be assumed as:

$$\mathbf{R}_{\text{edge}} = \begin{pmatrix} M_x \\ M_y \\ M_{xy} \\ T_x \\ T_y \end{pmatrix} = \mathbf{R}^0 + \mathbf{R}^* + \mathbf{R}^f = \sum_{i=1}^k \mathbf{R}_i^0 \beta_i + \mathbf{R}^* + \sum_{j=1}^2 \mathbf{R}_j^f \alpha_j \quad (22)$$

with:

$$\mathbf{R}_j^f = \begin{pmatrix} M_{xj}^f \\ M_{yj}^f \\ M_{xyj}^f \\ T_{xj}^f \\ T_{yj}^f \end{pmatrix} = \begin{pmatrix} -(1-\mu)D \frac{\partial^2 f_j}{\partial x \partial y} \\ (1-\mu)D \frac{\partial^2 f_j}{\partial x \partial y} \\ -\frac{1}{2}(1-\mu)D \left( \frac{\partial^2 f_j}{\partial y^2} - \frac{\partial^2 f_j}{\partial x^2} \right) \\ -C \frac{\partial f_j}{\partial y} \\ C \frac{\partial f_j}{\partial x} \end{pmatrix}, (j=1, 2) \quad (23)$$

The detailed expressions of the resultants derived from  $f$  are given in Table II (Shang *et al.*, 2015). It is shown that, these resultants are exponentially distributed as the direction perpendicular to the SS1 or the FREE edge, while no exponential distributions exist along the direction parallel to the SS1 or FREE edge.

$\mathbf{R}_j^f$	$j = 1$	$j = 2$
$M_{xj}^f$	$(1-\mu)mne^{mx+ny-a_0}$	$(1-\mu)[(nx-my)mn+n^2-m^2]e^{mx+nty-a_0}$
$M_{yj}^f$	$-(1-\mu)mne^{mx+ny-a_0}$	$-(1-\mu)[(nx-my)mn+n^2-m^2]e^{mx+nty-a_0}$
$M_{xyj}^f$	$\frac{1}{2}(1-\mu)(n^2-m^2)e^{mx+ny-a_0}$	$\frac{1}{2}(1-\mu)[-4mn+(nx-my)(n^2-m^2)]e^{mx+nty-a_0}$
$T_{xj}^f$	$\frac{C}{D}ne^{mx+ny-a_0}$	$\frac{C}{D}[(nx-my)n-m]e^{mx+nty-a_0}$
$T_{yj}^f$	$-\frac{C}{D}me^{mx+ny-a_0}$	$-\frac{C}{D}[(nx-my)m+n]e^{mx+nty-a_0}$

Eight-node elements

**Table II.**  
Two analytical solutions for the displacement function  $f$  and the resulting resultant forces

To formulate the elements HDF-P8-SS1 (with SS1 edge effects) and HDF-P8-FREE (with free edge effects), the modified general solution part  $\mathbf{S}_{\text{mod}}^{\text{edge}}$  and the modified particular solution part  $\mathbf{R}_{\text{mod}}^{\text{edge}}$  when the plate is subjected to a uniformly distributed transverse load  $q$  are needed.

Element HDF-P8-SS1 or HDF-P8-FREE should be allocated along the SS1 or FREE edge of the plate (for example, Edge 12 in [Figure 2](#)). The boundary resultant force vector at Edge 12 should satisfy the following SS1 or FREE boundary conditions:

$$\bar{\mathbf{R}}_{\text{edge}} = \mathbf{L}_{\text{edge}} \mathbf{R}_{\text{edge}} = \mathbf{0} \quad (24)$$

where:

$$\begin{cases} \bar{\mathbf{R}}_{\text{SS1}} = \left\{ \frac{\bar{M}_n}{\bar{M}_{ns}} \right\}_{\text{SS1}} \\ \bar{\mathbf{R}}_{\text{FREE}} = \left\{ \frac{\bar{M}_n}{\bar{T}_n} \right\}_{\text{FREE}} \end{cases} \quad (25)$$

$$\begin{cases} \mathbf{L}_{\text{SS1}} = \begin{bmatrix} l_x^2 & l_y^2 & 2l_x l_y & 0 & 0 \\ -l_x l_y & l_x l_y & l_x^2 - l_y^2 & 0 & 0 \end{bmatrix}_{\text{SS1}} \\ \mathbf{L}_{\text{FREE}} = \begin{bmatrix} l_x^2 & l_y^2 & 2l_x l_y & 0 & 0 \\ -l_x l_y & l_x l_y & l_x^2 - l_y^2 & 0 & 0 \\ 0 & 0 & 0 & l_x & l_y \end{bmatrix}_{\text{FREE}} \end{cases} \quad (26)$$

$$\begin{cases} \mathbf{R}_{\text{SS1}} = \mathbf{S}_{\Delta}^{\text{SS1}} \boldsymbol{\beta}_{\Delta}^{\text{SS1}} + \mathbf{S}_{\nabla}^{\text{SS1}} \boldsymbol{\beta}_{\nabla}^{\text{SS1}} + \mathbf{R}^* \\ \mathbf{R}_{\text{FREE}} = \mathbf{S}_{\Delta}^{\text{FREE}} \boldsymbol{\beta}_{\Delta}^{\text{FREE}} + \mathbf{S}_{\nabla}^{\text{FREE}} \boldsymbol{\beta}_{\nabla}^{\text{FREE}} + \mathbf{R}^* \end{cases} \quad (27)$$

in which:

$$\begin{cases} \mathbf{S}_{\Delta}^{\text{SS1}} = [\mathbf{R}_1^0 \dots \mathbf{R}_{10}^0 \mathbf{R}_{13}^0 \mathbf{R}_{15}^0 \mathbf{R}_{17}^0 \dots \mathbf{R}_{23}^0] \\ \mathbf{S}_{\Delta}^{\text{FREE}} = [\mathbf{R}_1^0 \dots \mathbf{R}_5^0 \mathbf{R}_7^0 \mathbf{R}_8^0 \mathbf{R}_9^0 \mathbf{R}_{11}^0 \mathbf{R}_{13}^0 \mathbf{R}_{14}^0 \mathbf{R}_{15}^0 \mathbf{R}_{19}^0 \mathbf{R}_{21}^0 \mathbf{R}_{22}^0 \mathbf{R}_{23}^0] \end{cases} \quad (28)$$

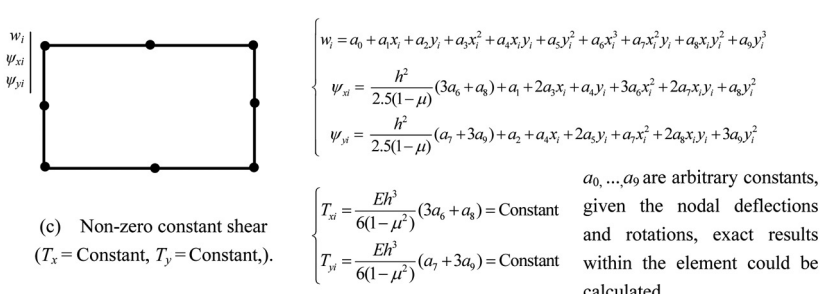
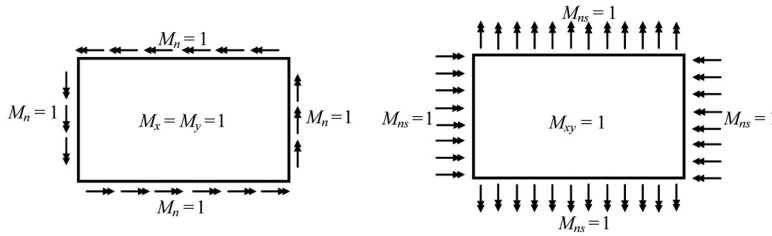
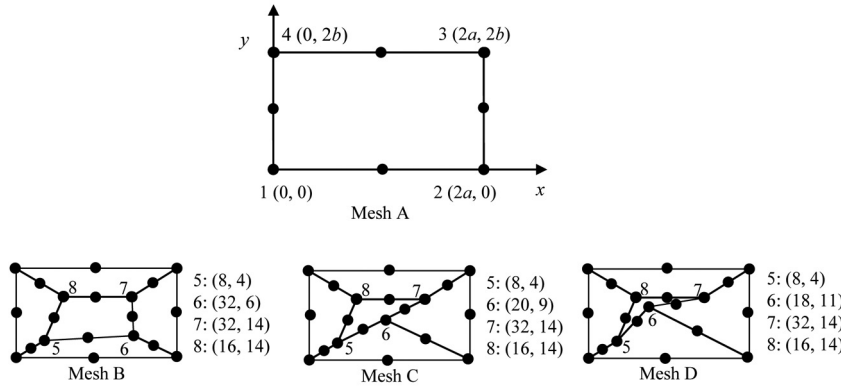
$$\begin{cases} \mathbf{S}_{\nabla}^{\text{SS1}} = [\mathbf{R}_{11}^0 \mathbf{R}_{12}^0 \mathbf{R}_{14}^0 \mathbf{R}_{16}^0 \mathbf{R}_1^f \mathbf{R}_2^f] \\ \mathbf{S}_{\nabla}^{\text{FREE}} = [\mathbf{R}_6^0 \mathbf{R}_{10}^0 \mathbf{R}_{12}^0 \mathbf{R}_{16}^0 \mathbf{R}_{17}^0 \mathbf{R}_{18}^0 \mathbf{R}_{20}^0 \mathbf{R}_1^f \mathbf{R}_2^f] \end{cases} \quad (29)$$

The detailed expressions of the matrices  $\mathbf{S}_{\Delta}^{\text{edge}}$  and  $\mathbf{S}_{\nabla}^{\text{edge}}$  can be obtained from [Tables I](#) and [II](#). Equations (28) to (29) are substituted into [equation \(27\)](#), three sets of constraint equations

$$E = 1000.0; \mu = 0.3; h = 0.04, 0.4, 4; a = 20; b = 10.$$

Eight-node elements

559



can be obtained by substituting the coordinates  $(x_1, y_1), (x_2, y_2), (x_5, y_5)$  of nodes 1, 2, 5 into equation (24):

$$\boldsymbol{\kappa}_{\Delta}^{\text{edge}} \boldsymbol{\beta}_{\Delta}^{\text{edge}} + \boldsymbol{\kappa}_{\nabla}^{\text{edge}} \boldsymbol{\beta}_{\nabla}^{\text{edge}} + \boldsymbol{\kappa}_{\Omega}^{\text{edge}} = \mathbf{0} \quad (30)$$

With:

Figure 3.  
Patch tests,  
geometry,  
loads and  
meshes

$$\left\{ \begin{array}{l} \boldsymbol{\kappa}_{\Delta}^{\text{SS1}} = \begin{bmatrix} \mathbf{L}_{\text{SSI}} \mathbf{S}_{\Delta}^{\text{SS1}}(x_1, y_1) \\ \mathbf{L}_{\text{SSI}} \mathbf{S}_{\Delta}^{\text{SS1}}(x_2, y_2) \\ \mathbf{L}_{\text{SSI}} \mathbf{S}_{\Delta}^{\text{SS1}}(x_5, y_5) \end{bmatrix}, \boldsymbol{\kappa}_{\nabla}^{\text{SS1}} = \begin{bmatrix} \mathbf{L}_{\text{SSI}} \mathbf{S}_{\nabla}^{\text{SS1}}(x_1, y_1) \\ \mathbf{L}_{\text{SSI}} \mathbf{S}_{\nabla}^{\text{SS1}}(x_2, y_2) \\ \mathbf{L}_{\text{SSI}} \mathbf{S}_{\nabla}^{\text{SS1}}(x_5, y_5) \end{bmatrix}, \boldsymbol{\kappa}_{\Omega}^{\text{SS1}} = \begin{bmatrix} \mathbf{L}_{\text{SSI}} \mathbf{R}^*(x_1, y_1) \\ \mathbf{L}_{\text{SSI}} \mathbf{R}^*(x_2, y_2) \\ \mathbf{L}_{\text{SSI}} \mathbf{R}^*(x_5, y_5) \end{bmatrix} \\ \boldsymbol{\kappa}_{\Delta}^{\text{FREE}} = \begin{bmatrix} \mathbf{L}_{\text{FREE}} \mathbf{S}_{\Delta}^{\text{FREE}}(x_1, y_1) \\ \mathbf{L}_{\text{FREE}} \mathbf{S}_{\Delta}^{\text{FREE}}(x_2, y_2) \\ \mathbf{L}_{\text{FREE}} \mathbf{S}_{\Delta}^{\text{FREE}}(x_5, y_5) \end{bmatrix}, \boldsymbol{\kappa}_{\nabla}^{\text{FREE}} = \begin{bmatrix} \mathbf{L}_{\text{FREE}} \mathbf{S}_{\nabla}^{\text{FREE}}(x_1, y_1) \\ \mathbf{L}_{\text{FREE}} \mathbf{S}_{\nabla}^{\text{FREE}}(x_2, y_2) \\ \mathbf{L}_{\text{FREE}} \mathbf{S}_{\nabla}^{\text{FREE}}(x_5, y_5) \end{bmatrix}, \boldsymbol{\kappa}_{\Omega}^{\text{FREE}} = \begin{bmatrix} \mathbf{L}_{\text{FREE}} \mathbf{R}^*(x_1, y_1) \\ \mathbf{L}_{\text{FREE}} \mathbf{R}^*(x_2, y_2) \\ \mathbf{L}_{\text{FREE}} \mathbf{R}^*(x_5, y_5) \end{bmatrix} \end{array} \right. \quad (31)$$

where  $\boldsymbol{\kappa}_{\Delta}^{\text{SS1}}$  is a  $6 \times 19$  matrix;  $\boldsymbol{\kappa}_{\nabla}^{\text{SS1}}$  is a  $6 \times 6$  matrix;  $\boldsymbol{\kappa}_{\Omega}^{\text{SS1}}$  is a  $6 \times 1$  matrix;  $\boldsymbol{\kappa}_{\Delta}^{\text{FREE}}$  is a  $9 \times 17$  matrix;  $\boldsymbol{\kappa}_{\nabla}^{\text{FREE}}$  is a  $9 \times 9$  matrix; and  $\boldsymbol{\kappa}_{\Omega}^{\text{FREE}}$  is a  $9 \times 1$  matrix. Then, the vector  $\boldsymbol{\beta}_{\nabla}^{\text{edge}}$  can be solved by:

$$\boldsymbol{\beta}_{\nabla}^{\text{edge}} = -\boldsymbol{\kappa}_{\nabla}^{\text{edge}^{-1}} (\boldsymbol{\kappa}_{\Delta}^{\text{edge}} \boldsymbol{\beta}_{\Delta}^{\text{edge}} + \boldsymbol{\kappa}_{\Omega}^{\text{edge}}) \quad (32)$$

Substitution of equation (32) into equation (27) yields:

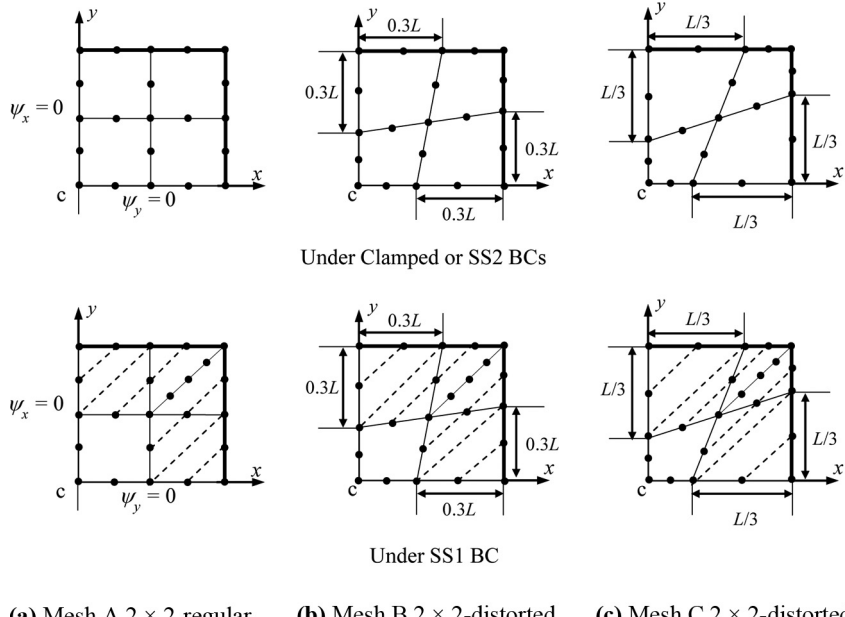


**Figure 4.**

Typical meshes used by a quarter of square plate (C is the central point of plate)



---


$$\mathbf{R}_{\text{edge}} = \mathbf{S}_{\text{mod}}^{\text{edge}} \boldsymbol{\beta}_{\Delta}^{\text{edge}} + \mathbf{R}_{\text{mod}}^{\text{edge}} \quad (33) \quad \text{Eight-node elements}$$

where:

$$\mathbf{S}_{\text{mod}}^{\text{edge}} = \mathbf{S}_{\Delta}^{\text{edge}} - \mathbf{S}_{\nabla}^{\text{edge}} \boldsymbol{\kappa}_{\nabla}^{\text{edge}^{-1}} \boldsymbol{\kappa}_{\Omega}^{\text{edge}} \quad (34)$$

$$\mathbf{R}_{\text{mod}}^{\text{edge}} = \mathbf{R}^* - \mathbf{S}_{\nabla}^{\text{edge}} \boldsymbol{\kappa}_{\nabla}^{\text{edge}^{-1}} \boldsymbol{\kappa}_{\Omega}^{\text{edge}} \quad (35)$$

561

**Equation (34)** is the final modified trial functions for resultants of element HDF-P8-SS1 or HDF-P8-FREE, which can satisfy the boundary conditions at the nodes along the SS1 or FREE edge.  $\mathbf{S}_{\text{mod}}^{\text{edge}}$  is the modified general solution part;  $\boldsymbol{\beta}_{\Delta}^{\text{edge}}$  is the final unknown coefficient vector;  $\mathbf{R}_{\text{mod}}^{\text{edge}}$  is the modified particular solution part when the plate is subjected to a uniformly distributed transverse load  $q$ .

To derive the formulations of the element HDF-P8-SS1 and the element HDF-P8-FREE, the  $\mathbf{S}$  and  $\mathbf{R}^*$  from [equations \(9\) to \(12\)](#) can be simply substituted by  $\mathbf{S}_{\text{mod}}^{\text{edge}}$  and  $\mathbf{R}_{\text{mod}}^{\text{edge}}$ , respectively. The other procedures are the same as the formulations of element HDF-P8-23 $\beta$ .

#### 4. Numerical examples

In this section, the performances of the proposed elements HDF-P8-23 $\beta$ , HDF-P8-SS1 and HDF-P8-FREE are fully assessed by some classic benchmark examples. Both traditional and new severely distorted meshes are used. Meanwhile, the results calculated by element S8R in [Abaqus \(2009\)](#), some other well-known high-order quadrilateral elements, and the

$h/L$	Mesh type	Mesh density					Analytical solutions
		1 × 1	2 × 2	4 × 4	8 × 8	16 × 16	
$10^{-30} \sim 0.001$	Mesh A-regular	0.12505	0.12636	0.12652	0.12653	0.12653	0.1265
	Mesh B-distorted	—	0.12634	0.12652	0.12653	0.12653	
	Mesh C-distorted	—	0.12628	0.12652	0.12653	0.12653	
0.01	Mesh A-regular	0.12530	0.12662	0.12677	0.12678	0.12678	0.1267
	Mesh B-distorted	—	0.12659	0.12677	0.12678	0.12678	
	Mesh C-distorted	—	0.12654	0.12677	0.12678	0.12678	
0.1	Mesh A-regular	0.14944	0.15072	0.15066	0.15055	0.15049	0.1499
	Mesh B-distorted	—	0.15071	0.15067	0.15056	0.15049	
	Mesh C-distorted	—	0.15066	0.15069	0.15057	0.15050	
$10^{-30} \sim 0.001$	Mesh A-regular	0.24196	0.22902	0.22908	0.22905	0.22905	0.2291
	Mesh B-distorted	—	0.22069	0.22895	0.22903	0.22905	
	Mesh C-distorted	—	0.21864	0.22879	0.22901	0.22905	
0.01	Mesh A-regular	0.24187	0.22909	0.22912	0.22910	0.22909	0.2291
	Mesh B-distorted	—	0.22137	0.22899	0.22908	0.22909	
	Mesh C-distorted	—	0.21935	0.22887	0.22907	0.22909	
0.1	Mesh A-regular	0.23827	0.23159	0.23214	0.23209	0.23203	0.231
	Mesh B-distorted	—	0.23118	0.23217	0.23210	0.23203	
	Mesh C-distorted	—	0.23061	0.23218	0.23211	0.23204	

**Table III.**  
Clamped square plate: dimensionless results of central deflection  $w_c/(qL^4/100D)$  and moment  $M_c/(qL^2/10D)$  obtained by element HDF-P8-23 $\beta$  (example 4.3)

low-order hybrid displacement function elements proposed by Cen *et al.* (2014) and Shang *et al.* (2015) are also given for comparison.

#### 4.1 Eigenvalues and rank

It is found that, for extremely thin- and moderately thick-plate cases, each element stiffness matrix of three new elements always produces only three zero eigenvalues corresponding to

$h/L$	Mesh type	Mesh density						Analytical solutions
		1 × 1	2 × 2	4 × 4	8 × 8	16 × 16		
$w_c/(qL^4/100D)$								
$10^{-30} \sim 0.001$	Mesh A-regular	0.40579	0.40620	0.40623	0.40623	0.40623	0.40623	0.4062
	Mesh B-distorted	—	0.40626	0.40623	0.40623	0.40623	0.40623	0.40623
	Mesh C-distorted	—	0.40628	0.40624	0.40623	0.40623	0.40623	0.40623
0.01	Mesh A-regular	0.40601	0.40641	0.40644	0.40644	0.40644	0.40644	0.4064
	Mesh B-distorted	—	0.40646	0.40644	0.40644	0.40644	0.40644	0.40644
	Mesh C-distorted	—	0.40648	0.40644	0.40644	0.40644	0.40644	0.40644
0.1	Mesh A-regular	0.42697	0.42724	0.42728	0.42728	0.42728	0.42728	0.4273
	Mesh B-distorted	—	0.42725	0.42728	0.42728	0.42728	0.42728	0.42728
	Mesh C-distorted	—	0.42726	0.42728	0.42728	0.42728	0.42728	0.42728
$M_c/(qL^2/10D)$								
$10^{-30} \sim 0.001$	Mesh A-regular	0.49074	0.47909	0.47888	0.47887	0.47886	0.47886	0.47886
	Mesh B-distorted	—	0.47384	0.47863	0.47883	0.47886	0.47886	0.47886
	Mesh C-distorted	—	0.47263	0.47841	0.47882	0.47886	0.47886	0.47886
0.01	Mesh A-regular	0.49060	0.47908	0.47888	0.47886	0.47886	0.47886	0.4789
	Mesh B-distorted	—	0.47416	0.47866	0.47884	0.47886	0.47886	0.47886
	Mesh C-distorted	—	0.47298	0.47849	0.47884	0.47886	0.47886	0.47886
0.1	Mesh A-regular	0.48279	0.47869	0.47884	0.47886	0.47886	0.47886	0.47886
	Mesh B-distorted	—	0.47818	0.47883	0.47886	0.47886	0.47886	0.47886
	Mesh C-distorted	—	0.47786	0.47883	0.47886	0.47886	0.47886	0.47886

**Table IV.** SS2 square plate: dimensionless results of central deflection  $w_c/(qL^4/100D)$  and moment  $M_c/(qL^2/10D)$  obtained by element HDF-P8-23 $\beta$  (example 4.3)

$h/L$	Mesh type	Mesh density						Analytical solutions
		1 × 1	2 × 2	4 × 4	8 × 8	16 × 16		
$w_c/(qL^4/100D)$								
$10^{-30} \sim 0.001$	Mesh A-regular	0.40925	0.40698	0.40678	0.40658	0.40631	0.4062	0.4062
	Mesh B-distorted	—	0.40691	0.40656	0.40648	0.40634	0.40634	0.40634
	Mesh C-distorted	—	0.40695	0.40657	0.40643	0.40637	0.40637	0.40637
0.1	Mesh A-regular	0.47047	0.46388	0.46220	0.46186	0.46187	0.46187	0.4617
	Mesh B-distorted	—	0.46265	0.46191	0.46181	0.46181	0.46181	0.46181
	Mesh C-distorted	—	0.46223	0.46182	0.46181	0.46181	0.46189	0.46189
$M_c/(qL^2/10D)$								
$10^{-30} \sim 0.001$	Mesh A-regular	0.44896	0.48035	0.47937	0.47917	0.47893	0.4789	0.4789
	Mesh B-distorted	—	0.47518	0.47896	0.47906	0.47895	0.47895	0.47895
	Mesh C-distorted	—	0.47420	0.47882	0.47900	0.47898	0.47898	0.47898
0.1	Mesh A-regular	0.45202	0.51146	0.50995	0.50972	0.50974	0.5096	0.5096
	Mesh B-distorted	—	0.50959	0.50970	0.50967	0.50974	0.50974	0.50974
	Mesh C-distorted	—	0.50909	0.50963	0.50968	0.50976	0.50976	0.50976

**Table V.** SS1 square plate: dimensionless results of central deflection  $w_c/(qL^4/100D)$  and moment  $M_c/(qL^2/10D)$  obtained by element HDF-P8-23 $\beta$  and HDF-P8-SS1 (example 4.3)

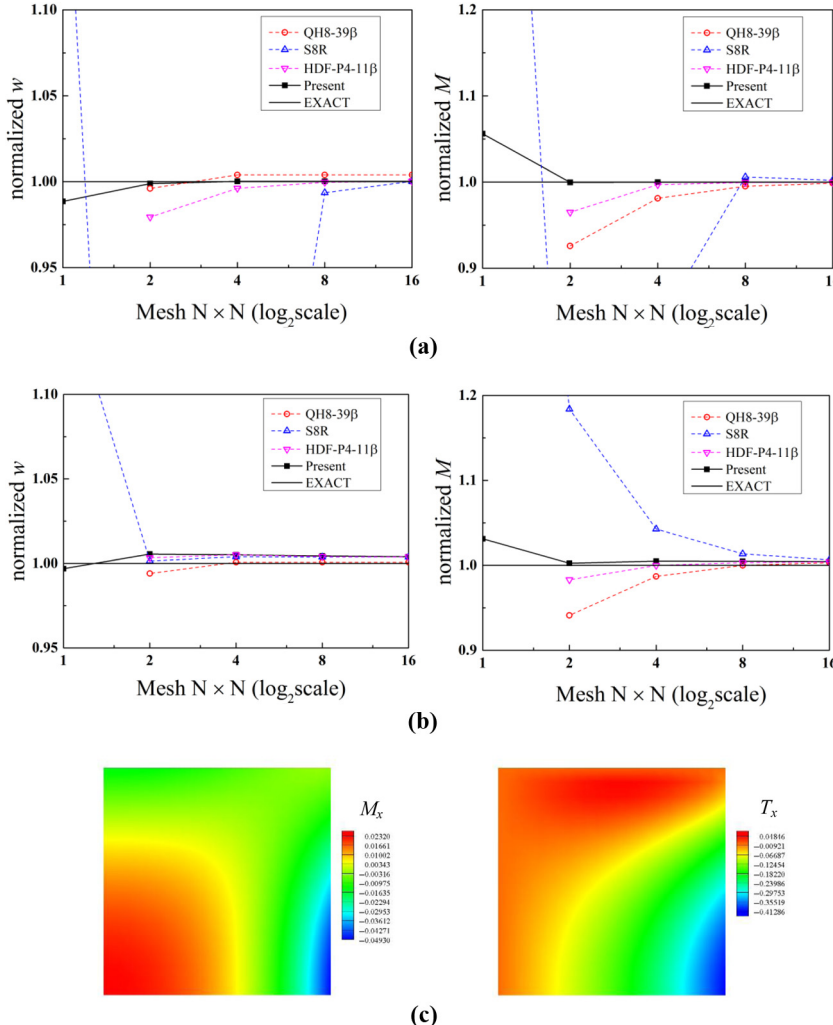
three rigid body modes for various regular or distorted element shapes. As a result, the proper rank and the absence of spurious modes can ensure that the proposed elements are stable.

Eight-node elements

#### 4.2 Patch tests for element HDF-P8-23 $\beta$

Figure 3 plots the Irons patch test problems. These tests are only performed for element HDF-P8-23 $\beta$  without edge effect. And different test conditions are summarized as follows:

563



**Notes:** (a)  $h/L = 0.001$  (thin-plate case); (b)  $h/L = 0.1$  (thick-plate case); (c) contour plot under  $h/L = 0.1$  using  $16 \times 16$  mesh

**Figure 5.** Convergence of the central deflections and moments and contour plot for square plates subjected to uniform load (clamped BC, Mesh A)

- (1) *Meshes*: Four mesh types are used. Mesh A contains only one eight-node element, while Meshes B, C and D are divided into five distorted elements.
- (2) *Loads and constraints*: Distributed line loads along the patch boundaries; three nodal deflections are constrained ( $w_1 = w_2 = w_3 = 0$ ) to eliminate rigid body motions.
- (3) *Span-thickness ratios*: Three different span-thickness ratios  $2a/h = 1,000, 100, 10$ , are considered:

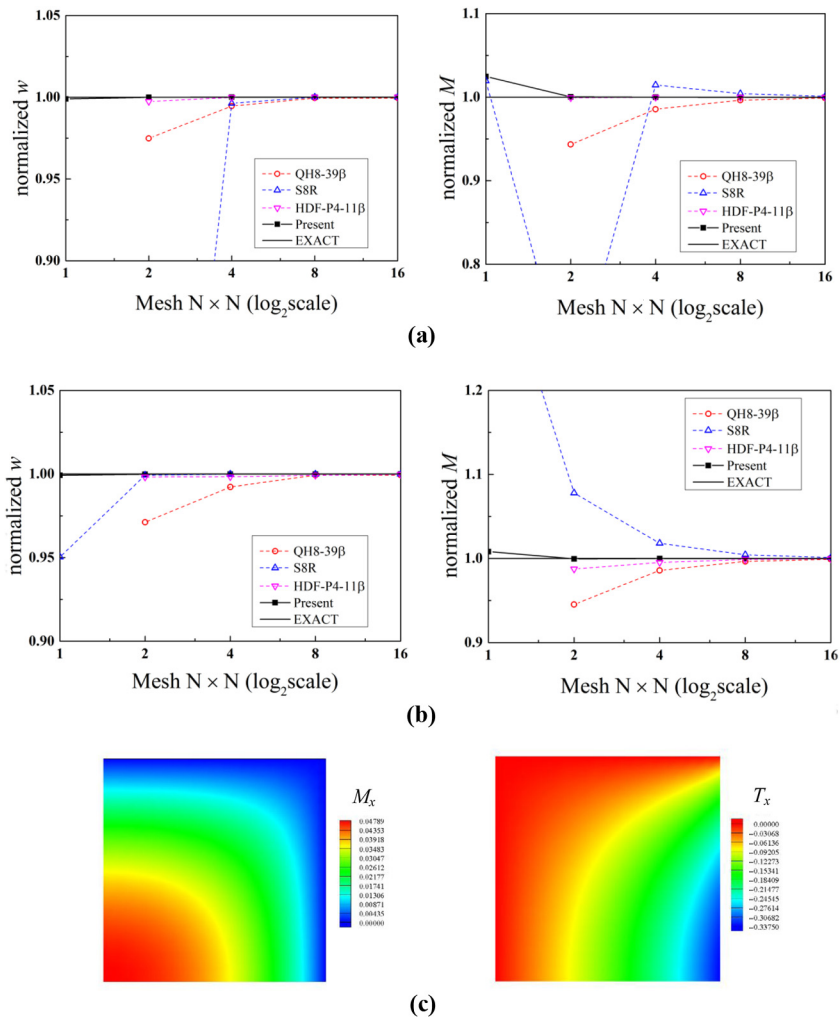
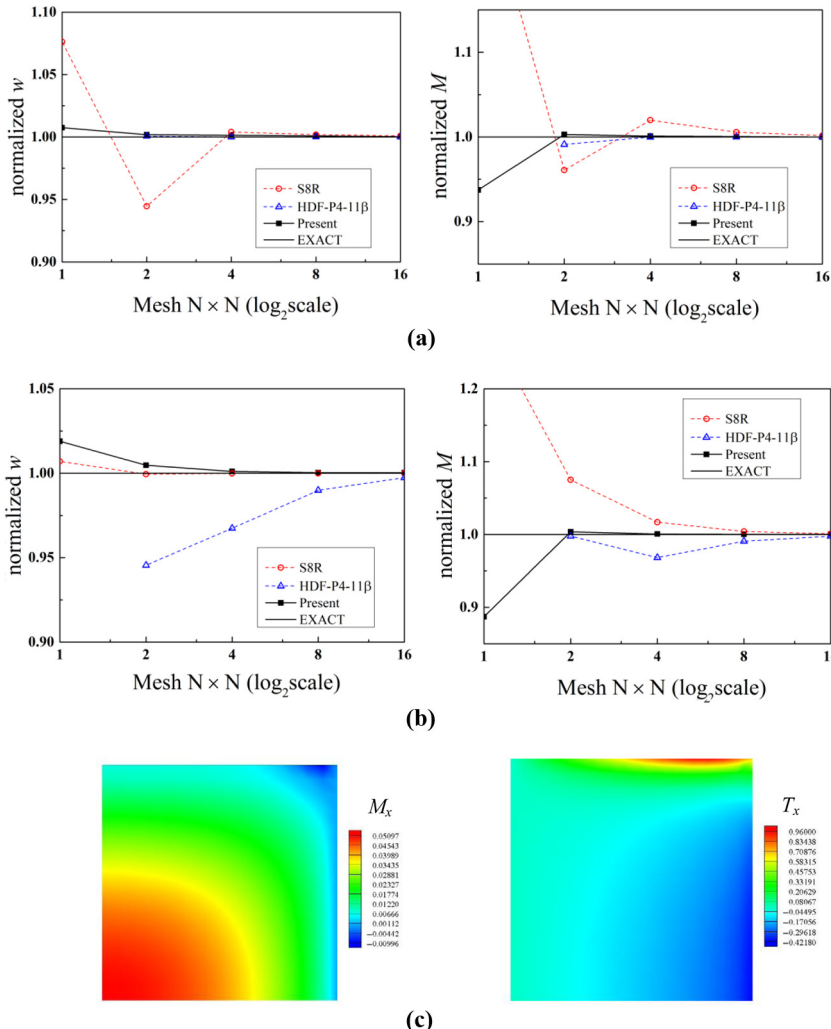


**Figure 6.**  
Convergence of the central deflections and moments and contour plot for square plates subjected to uniform load (SS2 BC, Mesh A)

**Notes:** (a)  $h/L = 0.001$  (thin-plate case); (b)  $h/L = 0.1$  (thick-plate case); (c) contour plot under  $h/L = 0.1$  using Mesh  $16 \times 16$

- *Constant bending moment case ( $M_n = 1$ ):* As shown in Figure 3a, the rectangular plate patch is subjected to bending moment  $M_n = 1$  along all its edges. The computed results of bending moments  $M_x (=1)$  and  $M_y (=1)$ , twisting moment  $M_{xy} (= 0)$ , shear forces  $T_x (= 0)$  and  $T_y (= 0)$ , at any point, are exact for all span–thickness ratio cases.
- *Constant twisting moment case ( $M_{ns} = 1$ ):* As shown in Figure 3b, the rectangular plate patch is subjected to twisting moment  $M_{ns} = 1$  along its



**Notes:** (a)  $h/L = 0.001$  (thin-plate case); (b)  $h/L = 0.1$  (thick-plate case); (c) contour plot under  $h/L = 0.1$  using Mesh  $16 \times 16$

**Figure 7.** Convergence of the central deflections and moments and contour plot for square plates subjected to uniform load (SS1 BC, mesh a)

four edges. In all cases, the numerical results of  $M_{xy}$  ( $= 1$ ),  $M_x$  ( $= 0$ ),  $M_y$  ( $= 0$ ),  $T_x$  ( $= 0$ ) and  $T_y$  ( $= 0$ ) obtained by the element HDF-P8-23 $\beta$  are exact.

- *Non-zero constant shear force case* ( $T_x = \text{Constant}$ ,  $T_y = \text{Constant}$ ). As shown in [Figure 3c](#), the eight boundary nodes of the rectangular plate patch are imposed by given deflections and rotations. The element HDF-P8-23 $\beta$  can give the exact constant shear force ( $T_x = \text{Constant}$ ,  $T_y = \text{Constant}$ ) corresponding to different span–thickness ratio cases.

#### 4.3 Square plate subjected to uniformly distributed load

[Figure 4](#) gives the meshes used for this example, in which only a quarter of the plate is considered owing to the biaxial symmetry. The geometric parameters and conditions are given as follows:

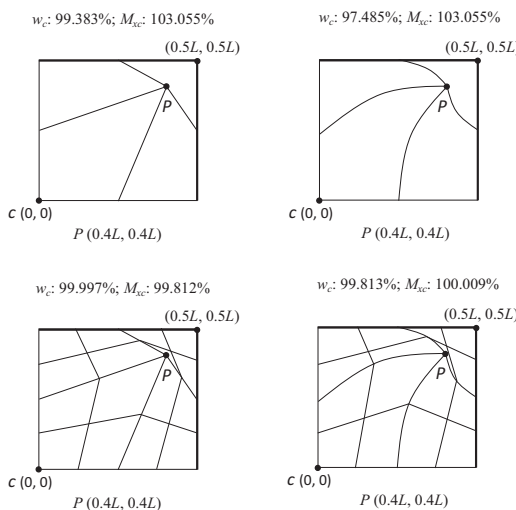


**Figure 8.**

Distorted meshes and normalized results for a quarter of clamped square plate (omitting middle nodes)

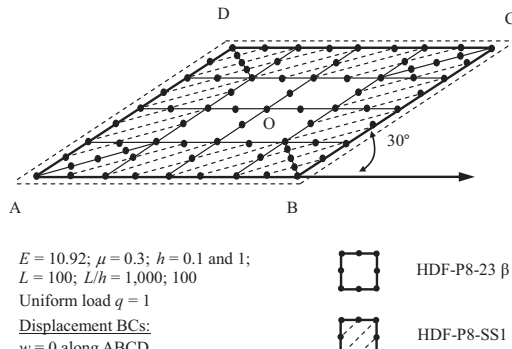


**Figure 9.**

Mesh  $4 \times 4$  for Morley's  $30^\circ$  skew plate

- *Geometric parameters:*  $L$  denotes the edge length;  $h$  denotes the thickness of the plate; Poisson's ratio  $\mu = 0.3$ .
- *Load and boundary conditions (BCs):* The square plate is subjected to a uniform transverse load  $q = 1$ . Three BC cases – the clamped BC ( $w = 0, \psi_n = 0, \psi_s = 0$ ), the soft simply supported (SS1) BC ( $w = 0$ ) and the hard simply supported (SS2) BC ( $w = 0, \psi_s = 0$ ) – are considered.

Eight-node elements

567

Mesh $N \times N$	$4 \times 4$	$8 \times 8$	$16 \times 16$	$32 \times 32$	Morley's solutions for thin plate
<i>(a) Central deflection <math>w_o/(qL^4/1000D)</math></i>					
QH8-39 $\beta$	0.416	0.422	0.420	0.417	0.408
HDF-P4-11 $\beta$	0.462	0.426	0.419	0.416	
S8R	0.181	0.279	0.326	0.356	
Present	0.423	0.419	0.417	0.415	
<i>(b) Central max principal moment <math>M_{\max}/(qL^2/100D)</math></i>					
QH8-39 $\beta$	1.911	1.936	1.938	1.933	1.910
HDF-P4-11 $\beta$	2.197	1.873	1.935	1.930	
S8R	1.241	1.517	1.671	1.757	
Present	1.932	1.902	1.925	1.925	
<i>(c) Central min principal moment <math>M_{\min}/(qL^2/100D)</math></i>					
QH8-39 $\beta$	0.966	1.136	1.131	1.122	1.080
HDF-P4-11 $\beta$	1.399	1.104	1.169	1.125	
S8R	0.492	0.705	0.802	0.889	
Present	1.121	1.109	1.119	1.112	

Sources: QH8-39 $\beta$  (Li et al., 2015); HDF-P4-11 $\beta$  (Cen et al., 2014); S8R (Abaqus, 2009); Morley (1963)

**Table VI.**  
Results of deflections  
and principal  
moments at the  
center of Morley's  
 $30^\circ$  skew plate  
( $L/h = 1,000$ )

Mesh $N \times N$	$4 \times 4$	$8 \times 8$	$16 \times 16$	$32 \times 32$	Morley's solutions for thin plate	3D solution
<i>(a) Central deflection <math>w_o/(qL^4/1000D)</math></i>						
QH8-39 $\beta$	0.418	0.425	0.425	0.424	0.408	0.423
HDF-P4-11 $\beta$	0.463	0.427	0.421	0.420		
S8R	0.262	0.328	0.377	0.406		
Present	0.427	0.425	0.424	0.424		
<i>(b) Central max principal moment <math>M_{\max}/(qL^2/100D)</math></i>						
QH8-39 $\beta$	1.919	1.941	1.950	1.954	1.910	
HDF-P4-11 $\beta$	2.198	1.882	1.942	1.937		
S8R	1.717	1.705	1.828	1.904		
Present	1.956	1.931	1.949	1.954		
<i>(c) Central min principal moment <math>M_{\min}/(qL^2/100D)</math></i>						
QH8-39 $\beta$	0.963	1.134	1.143	1.143	1.080	
HDF-P4-11 $\beta$	1.400	1.108	1.157	1.130		
S8R	0.777	0.818	0.964	1.076		
Present	1.148	1.144	1.146	1.144		

Sources: QH8-39 $\beta$  (Li et al., 2015); HDF-P4-11 $\beta$  (Cen et al., 2014); S8R (Abaqus, 2009); Morley (1963); 3D (Babuška and Scapolla, 1989)

**Table VII.**  
Results of deflections  
and principal  
moments at the  
center of Morley's  
 $30^\circ$  skew plate  
( $L/h = 100$ )

- *Span-thickness ratios:* From a thick case ( $h/L = 0.1$ ) to a very thin case ( $h/L = 10^{-30}$ ).
- *Meshes:* Three mesh types are used, and the mesh densities are  $1 \times 1$ ,  $2 \times 2$ ,  $4 \times 4$ ,  $8 \times 8$  and  $16 \times 16$ .

The dimensionless results (here, let  $L = 1$  and  $D = 1$ ) of deflections and moments at the plate center are presented in Tables III to V. It should be noted that under SS1 BC, the edge effect will take place. So, as shown in Figure 4, element HDF-P8-SS1 will be allocated along the SS1 boundary, in which the corner region is split into two degenerated triangular elements. Because the shapes of the present elements are quite free, such meshes will not bring an

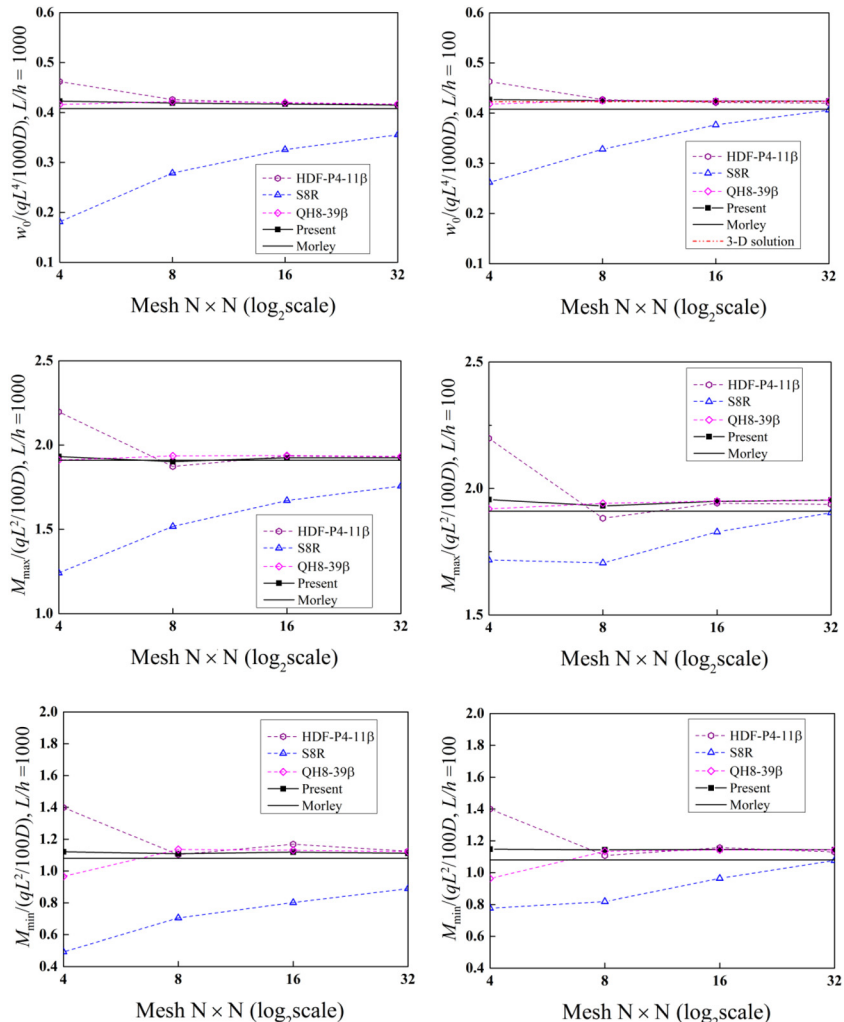
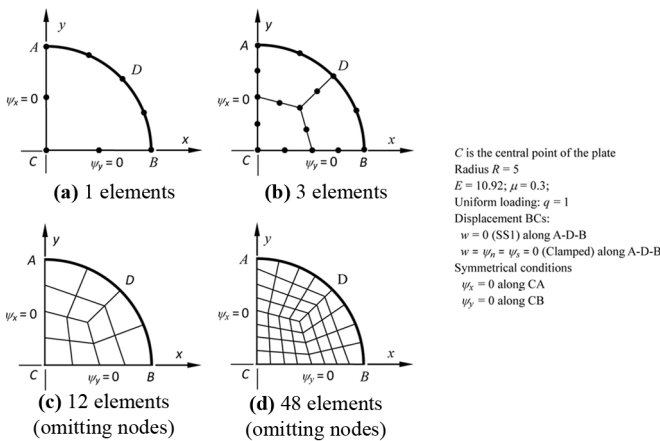


**Figure 10.**

Convergence test for central deflections and principle moments of Morley's 30° skew plate



**Notes:** (a) 1 elements; (b) 3 elements; (c) 12 elements (omitting nodes); (d) 48 elements (omitting nodes)

Figure 11.  
Circular plate  
problem

Mesh $N$	1	3	12	48	Analytical
(a) $h/R = 0.02$ ( $h = 0.1$ ) $w_c/w_{ref}$					
DONEA	0.9690	0.9980	0.9997	—	1.0000
Kuang	—	0.9945	0.9967	0.9992	(the reference value is 39831.5)
QH-39 $\beta$	—	1.0276	1.0075	1.0025	
S8R	0.9524	1.0070	0.9998	1.0000	
HDF-P4-11 $\beta$	—	1.0242	1.0065	1.0017	
Present	1.0002	1.0008	1.0001	1.0000	
$M_c/M_{ref}$					
Kuang	—	0.9864	0.9922	0.9961	1.0000
QH-39 $\beta$	—	0.9149	0.9922	0.9990	(the reference value is 5.15625)
S8R	1.1000	1.2424	1.0087	1.0027	
HDF-P4-11 $\beta$	—	1.0262	1.0046	1.0012	
Present	1.0152	1.0041	1.0003	1.0000	
(b) $h/R = 0.2$ ( $h = 1$ ) $w_c/w_{ref}$					
Kuang	—	0.9907	0.9975	0.9988	1.0000
QH-39 $\beta$	—	1.0841	1.0312	1.0120	(the reference value is 41.5994)
S8R	0.9594	1.0012	0.9999	1.0000	
HDF-P4-11 $\beta$	—	1.0206	1.0048	1.0010	
Present	1.0002	1.0010	1.0001	1.0000	
$M_c/M_{ref}$					
Kuang	—	0.9864	0.9922	0.9981	1.0000
QH-39 $\beta$	—	0.8408	0.9920	0.9990	(the reference value is 5.15625)
S8R	1.1468	1.0771	1.0156	1.0040	
HDF-P4-11 $\beta$	—	1.0170	1.0030	1.0007	
Present	1.0060	1.0008	1.0000	1.0000	

Table VIII.

Normalized center deflection  $w_c/w_{ref}$  and moments  $M_c/M_{ref}$  of simply supported (SS1) circular plates subjected to a uniform load

**Sources:** DONEA (Donea and Lamain, 1987); Kuang (Zhang and Kuang, 2007); QH-39 $\beta$  (Li et al., 2015); HDF-P4-11 $\beta$  (Cen et al., 2014); S8R (Abaqus, 2009)

unfavorable influence. The corresponding results are given in [Tables III to V](#), and plotted in [Figures 5 to 7](#). From [Figures 5\(c\), 6\(c\) and 7\(c\)](#), the distributions of the bending moments and the shear forces under different boundary conditions are clearly visualized. And the influence of the edge effects for shear force  $T_x$  can be observed in [Figure 7\(c\)](#). The new elements exhibit excellent performance for both precision and convergence for this example.

#### *4.4 Test for checking the sensitivity problem to mesh distortions*

As shown in [Figure 8](#), several distorted meshes are designed to test the sensitivity to mesh distortions for the new element HDF-P8-23 $\beta$ . A quarter of a thin square plate with symmetry and clamped boundary conditions is subjected to a uniformly distributed load. All parameters are the same as those given in Section 4.3.

The normalized results of the central deflection and moment of the plate are also given in [Figure 8](#). It can be seen that element HDF-P8-23 $\beta$  is quite robust even when the mesh is severely distorted.

#### *4.5 Skew plates subjected to uniformly distributed load*

[Figure 9](#) shows a new 4- × 4-mesh configuration and the geometric parameters for a 30° skew plate with SS1 BC (soft simply supported). This example has been studied by [Morley \(1963\)](#) under the thin-plate assumptions. Two characters exist in this test:

- (1) singularity appears in the bending moment at the obtuse corner; and
- (2) edge effect appears.

Mesh N	1	3	12	48	Analytical
(a) h/R = 0.02 (h = 0.1) $w_c/w_{ref}$					
DONEA	0.2960	1.0130	1.0020	—	1.0000
S8R	0.1042	0.8621	0.9619	0.9971	(the reference value is 9783.48)
Kuang	—	0.9620	0.9957	0.9998	
HDF-P4-11 $\beta$	—	0.7985	0.9484	0.9871	
Present	0.9965	0.9983	0.9999	1.0000	
$M_c/M_{ref}$					
S8R	0.1599	0.8169	1.0082	1.0083	1.0000
Kuang	—	0.9901	0.9951	0.9999	(the reference value is 2.03125)
HDF-P4-11 $\beta$	—	0.9151	0.9727	0.9933	
Present	1.0557	1.0050	1.0008	1.0001	
(b) h/R = 0.2 (h = 1) $w_c/w_{ref}$					
S8R	0.9698	0.9992	0.9993	1.0000	1.0000
Kuang	—	0.9931	0.9955	0.9974	(the reference value is 11.5513)
HDF-P4-11 $\beta$	—	0.8200	0.9512	0.9871	
Present	0.9984	0.9985	0.9999	1.0000	
Normalized center deflection $w_c/w_{ref}$ and moments $M_c/M_{ref}$ of clamped circular plates subjected to a uniform load					
Sources: DONEA ( <a href="#">Donea and Lamain, 1987</a> ); Kuang ( <a href="#">Zhang and Kuang, 2007</a> ); QH8-39 $\beta$ ( <a href="#">Li et al., 2015</a> ); HDF-P4-11 $\beta$ ( <a href="#">Cen et al., 2014</a> ); S8R ( <a href="#">Abaqus, 2009</a> );					

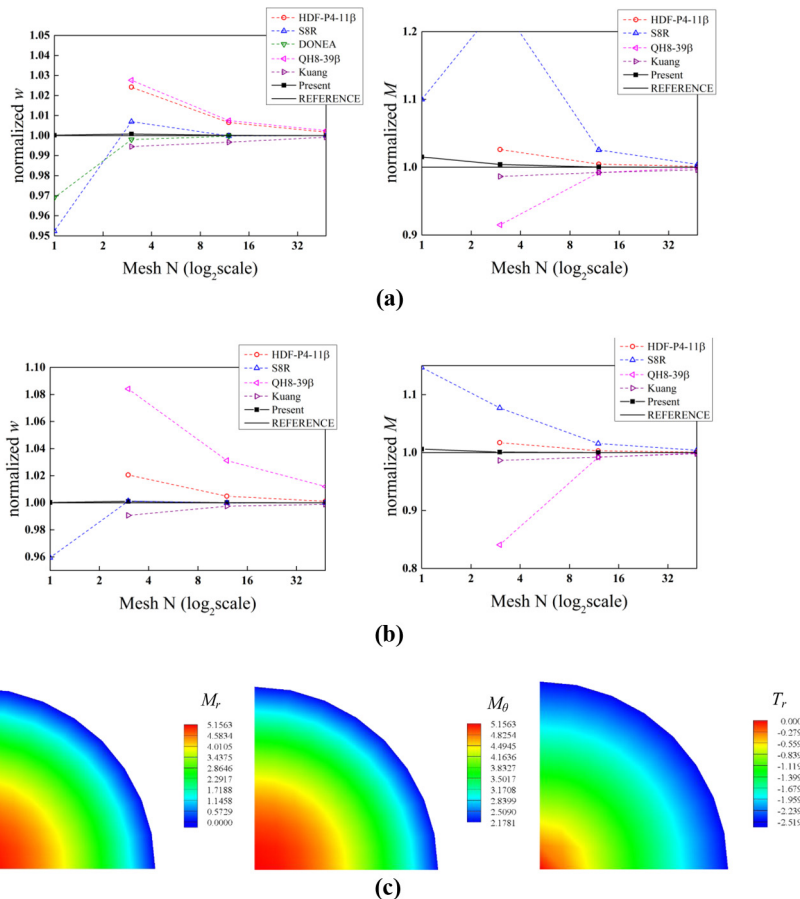
**Table IX.**

Normalized center deflection  $w_c/w_{ref}$  and moments  $M_c/M_{ref}$  of clamped circular plates subjected to a uniform load

This problem has also been solved as a 3D elastic case by Babuška and Scapolla (1989). Two span–thickness ratios ( $L/h = 1000, 100$ ) are considered. The principal bending moments and deflections at the central node O are calculated. Tables VI to VII and Figure 10 present the dimensionless results obtained by the new elements HDF-P8-23 $\beta$  and HDF-P8-SS1 (owing to the occurrence of the edge effects) and other models. Better convergence can be obtained by the new models when compared to other elements.

#### 4.6 Circular plate subjected to uniformly distributed load

Figure 11 shows a circular plate subjected to a uniform load  $q = 1$ . According to the symmetry, only a quarter of the plate is modeled. Two different thickness-radius ratio cases ( $h/R = 0.02, 0.2$ ), and two different BC cases, the soft simply supported (SSI) BC ( $w = 0$ ) and



**Notes:** (a)  $h/R = 0.02$  (thin-plate case); (b)  $h/R = 0.2$  (thick-plate case); (c) contour plot under  $h/R = 0.2$  using 48 elements

**Figure 12.**  
Convergence of the central deflections and moments and contour plot for circular plates subjected to uniform load (SSI BC)

the clamped BC ( $w = 0$ ,  $\psi_n = 0$ ,  $\psi_s = 0$ ), are considered. The analytical solutions can be found in references (Ayad *et al.*, 1998; Ayad and Rigolot, 2002). Results obtained by the new element HDF-P8-23 $\beta$  and some other models are given in Tables VIII to IX and plotted in Figures 12 and 13.

Because HDF-P8-23 $\beta$  is a high-order element with mid-side nodes, it is possible for the element to simulate the circular arc. This example can be perfectly solved by only using one HDF-P8-23 $\beta$  element, which cannot be achieved by other models in different literatures. Although the test contains the SS1 boundary condition, according to the Mindlin–Reissner theory, the edge effects will not take place in the circular plate case. So, satisfactory solutions can be obtained by using element HDF-P8-23 $\beta$  only.

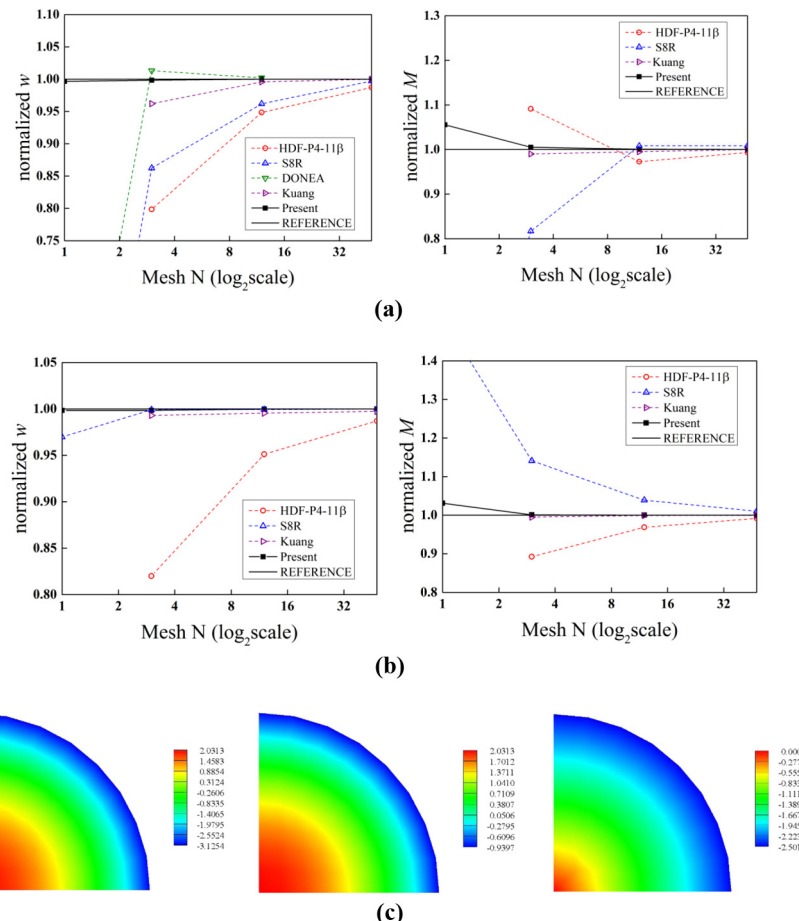


**Figure 13.**  
Convergence of the central deflections and moments and contour plot for circular plates subjected to uniform load (clamped BC)

**Notes:** (a)  $h/R = 0.02$  (thin-plate case); (b)  $h/R = 0.2$  (thick-plate case); (c) contour plot under  $h/R = 0.2$  using 48 elements

#### 4.7 Edge effect test

As shown in Figure 14, a square plate is subjected to a uniformly transverse load  $q$ . Because of symmetry, only one-quarter of the plate, ABCD (C is the center of the plate), is analyzed. Two boundary condition cases are studied:

- (1) SFSF, two opposite edges hard simply supported (SS2) and the other two edges free.
- (2) SS\*SS\*, two opposite edges hard simply supported (SS2) and the other two edges soft simply supported (SS1).

The edge length of the square plate is  $a$ , the thickness is  $h$  and the Poisson's ratio  $\mu = 0.3$ . Only one span–thickness ratio,  $a/h = 50$ , is considered.

Kant and Hinton (1983), (Kant and Gadgil, 2002) have solved the case by using the segmentation method. Thus, their solutions are presented here for comparison. Furthermore, results obtained by some other four-, five- and eight-node quadrilateral plate elements, including Shang *et al.* (2015), S4 (*Abaqus*, 2009), S8R (*Abaqus*, 2009), HMP15 (Saleeb and Chang, 1987) and CL8 (Spilker, 1982), are also presented for comparison.

**4.7.1 The SFSF plate.** The meshes and the locations of the elements HDF-P8-Free and HDF-P8-23 $\beta$  are also illustrated in Figure 14. The values of displacements and resultants at selected points, obtained by present method and Shang *et al.* (2015), Abaqus elements S8R (*Abaqus*, 2009), are listed in Table X for comparing the convergence rate. The results derived by two semi-analytic methods, including the segmentation method (Kant and Gadgil, 2002; Kant and Hinton, 1983) and the FEMOL (Yuan, 1993), are also presented.

The distributions of the resultants obtained by the present scheme along selected paths and the corresponding contour plots of the resultants are plotted through Figures 15 to 16. The values at nodes are smoothed solutions by averaging direct nodal values at all connective elements.

Figure 15 plots the distribution of  $T_x$  along the symmetry edge DC. Figure 16 shows the distributions of  $M_{xy}$  and  $T_y$  along the hard simply supported edge AB. Their distributions

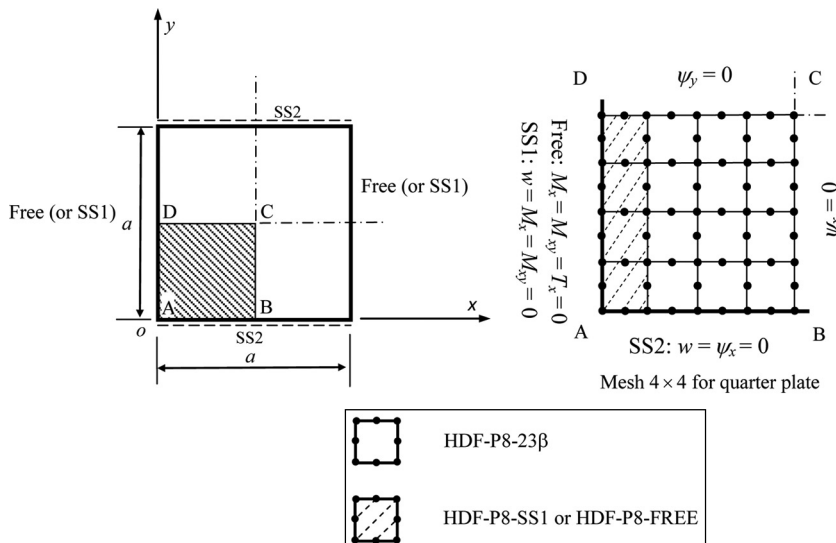
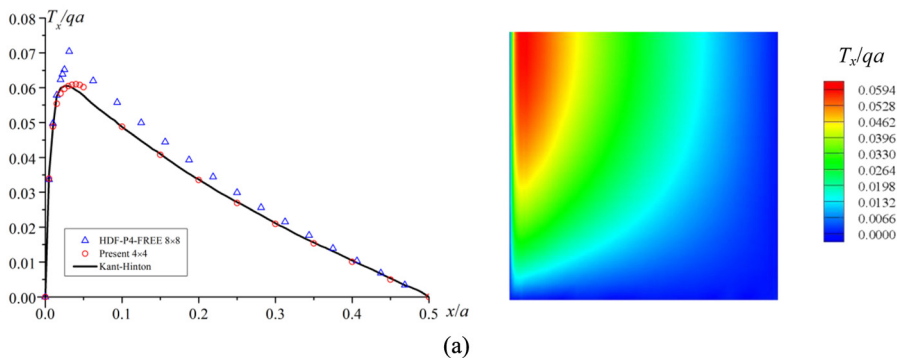
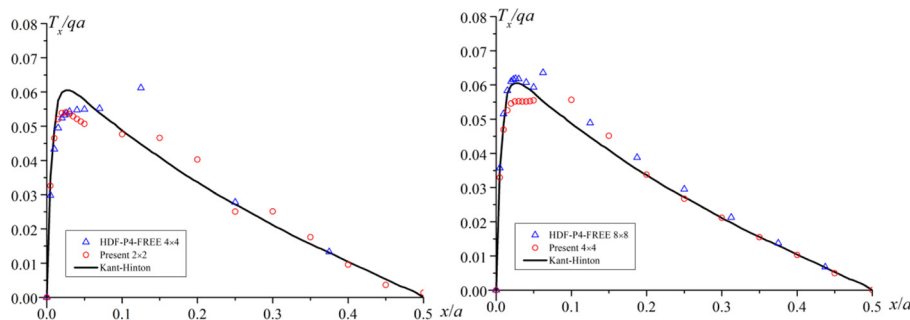


**Figure 14.**  
The typical meshes and the arrangement for the square plate with two opposite edges hard simply supported (SS2) and the other two free or soft simply supported (SS1)

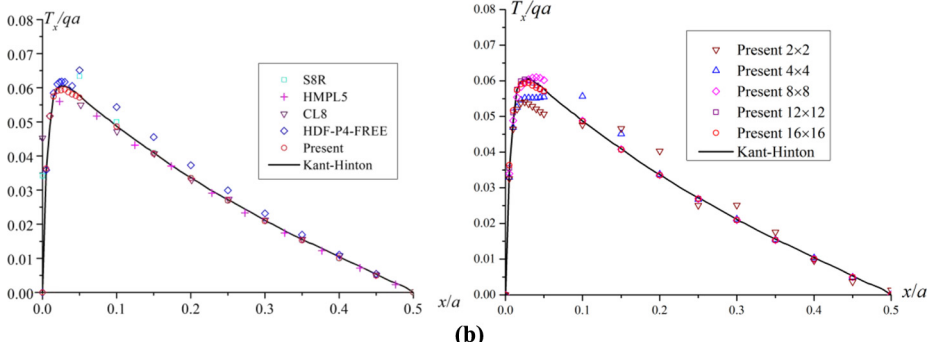
	Mesh $N \times N$	2 × 2	4 × 4	8 × 8	12 × 12	16 × 16	FEMOL	Kant
$\frac{w_C \cdot D}{qa^4}$								
HDF-P4-FREE								
	–	0.01311	0.01311	0.01311	0.01311	0.01311	0.01311	0.0131
S8R	0.01311	0.01311	0.01311	0.01311	0.01311	0.01311		
Present	0.01311	0.01311	0.01311	0.01311	0.01311	0.01311		
$\frac{w_D \cdot D}{qa^4}$								
HDF-P4-FREE								
	–	0.01507	0.01507	0.01507	0.01507	0.01507	0.01507	0.0150
S8R	0.01512	0.01507	0.01507	0.01507	0.01507	0.01507		
Present	0.01507	0.01507	0.01507	0.01507	0.01507	0.01507		
$\frac{M_{xC}}{qa^2}$								
HDF-P4-FREE								
	–	0.02650	0.02675	0.02680	0.02681	0.02683	0.0268	
S8R	0.02851	0.02731	0.02695	0.02688	0.02686			
Present	0.02576	0.02656	0.02676	0.02680	0.02681			
$\frac{M_{yC}}{qa^2}$								
HDF-P4-FREE								
	–	0.1229	0.1226	0.1225	0.1225	0.1225	0.1225	0.1220
S8R	0.1273	0.1237	0.1228	0.1226	0.1226			
Present	0.1235	0.1227	0.1225	0.1225	0.1225			
$\frac{M_{yC}}{qa^2}$								
HDF-P4-FREE								
	–	0.1304	0.1304	0.1304	0.1304	0.1304	0.1304	0.130
S8R	0.1361	0.1322	0.1312	0.1309	0.1308			
Present	0.1308	0.1305	0.1304	0.1304	0.1304			
$\frac{M_{xyA}}{qa^2}$								
HDF-P4-FREE								
	–	0.00000	0.00000	0.00000	0.00000	0.00000	NA	NA
S8R	0.01676	0.01795	0.01415	0.01124	0.00910			
Present	0.00000	0.00000	0.00000	0.00000	0.00000			
$\frac{T_{yB}}{qa}$								
HDF-P4-FREE								
	–	0.4381	0.4552	0.4609	0.4634	0.4679	0.463	
S8R	0.4286	0.4286	0.4678	0.4679	0.4679			
Present	0.4431	0.4612	0.4659	0.4671	0.4675			
$\frac{T_{xB}}{qa}$								
HDF-P4-FREE								
	–	0.00000	0.00000	0.00000	0.00000	0.00000	NA	NA
S8R	0.01362	0.04750	0.03875	0.03053	0.02468			
Present	0.00000	0.00000	0.00000	0.00000	0.00000			

**Table X.**  
The dimensionless results of displacements and resultants at certain positions for the SFSF square plate

**Sources:** FEMOL (Yuan, 1993); Kant (Kant and Gadgil, 2002; Kant and Hinton, 1983); HDF-P4-FREE (Shang *et al.*, 2015); S8R (Abaqus, 2009)



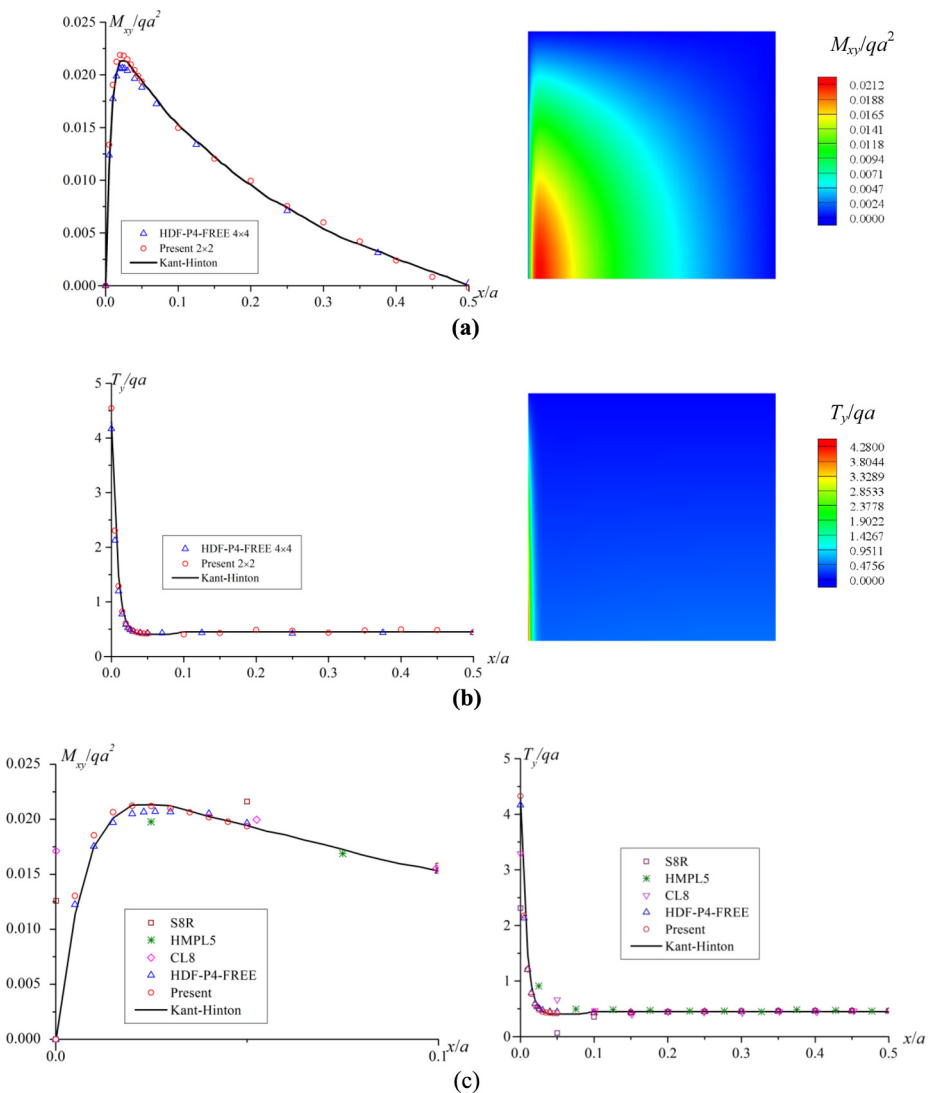
(a)



(b)

**Notes:** (a) Distributions of the shear force  $T_x$  along the symmetric edge CD ( $y = 0.5a$ ) with i)  $2 \times 2$  mesh; ii)  $4 \times 4$  mesh; iii)  $8 \times 8$  mesh; and iv) convergent contour plot with  $8 \times 8$  mesh; (b) i) comparisons of distributions of the shear force  $T_x$  along the symmetric edge CD ( $y = 0.5a$ ) with other methods with  $10 \times 10$  mesh; ii) convergence of the present method

**Figure 15.**  
Distributions,  
contour plots and  
comparisons of the  
shear force  $T_x$  for the  
SFSF case

**Figure 16.**

Distributions, contour plots and comparisons of the twisting moment  $M_{xy}$  and the shear force  $T_y$  for the SFSF case

**Notes:** (a) i) Distributions of the twisting moment  $M_{xy}$  along the hard simply supported edge AB ( $y = 0$ ) with  $2 \times 2$  mesh; ii) convergent contour plot with  $8 \times 8$  mesh; (b) i) distributions of the shear force  $T_y$  along the hard simply supported edge AB ( $y = 0$ ) with  $2 \times 2$  mesh; ii) convergent contour plot with  $8 \times 8$  mesh; c) i) comparisons of distributions of the twisting moment  $M_{xy}$ ; ii) Comparisons of distributions of the shear force  $T_y$  along the hard simply supported edge AB ( $y = 0$ ) with  $10 \times 10$  mesh

recalculated by the present method using a  $10 \times 10$  mesh, and results of some other quadrilateral plate elements are also given for comparison.

From the numerical results, some conclusions could be drawn:

- Compared to other elements, the combination of HDF-P8-Free and HDF-P8- $23\beta$  exhibits better prediction and convergence for the resultants. Meanwhile, for present elements, only a coarse mesh is enough to ensure that the zero resultant conditions are satisfied at the nodes along free edge.
- Compared to the low-order element proposed by [Shang et al. \(2015\)](#), the present element combination shows better performance in capturing the peak value of the resultants.

Mesh $N \times N$	$2 \times 2$	$4 \times 4$	$8 \times 8$	$12 \times 12$	$16 \times 16$	Kant
$\frac{w_c \cdot D}{qa^4}$						
HDF-P4-SS1	—	0.00410	0.00410	0.00410	0.00411	0.0041
S8R	0.00412	0.00411	0.00411	0.00411	0.00411	
Present	0.00411	0.00411	0.00411	0.00411	0.00411	
$\frac{M_{xc}}{qa^2}$						
HDF-P4-SS1	—	0.04806	0.04809	0.04810	0.04811	0.0481
S8R	0.05193	0.04901	0.04834	0.04822	0.04818	
Present	0.04814	0.04812	0.04813	0.04813	0.04813	
$\frac{M_{yc}}{qa^2}$						
HDF-P4-SS1	—	0.04821	0.04822	0.04824	0.04825	0.0482
S8R	0.05253	0.04913	0.04848	0.04836	0.04832	
Present	0.04815	0.04827	0.04827	0.04827	0.04827	
$\frac{M_{xyA}}{qa^2}$						
HDF-P4-SS1	—	0.00000	0.00000	0.00000	0.00000	NA
S8R	-0.02648	-0.02547	-0.01941	-0.01528	-0.01232	
Present	0.00000	0.00000	0.00000	0.00000	0.00000	
$\frac{T_{yA}}{qa}$						
HDF-P4-SS1	—	-5.087	-5.074	-5.047	-5.039	-5.214
S8R	-0.772	-1.325	-2.207	-2.834	-3.289	
Present	-5.504	-5.441	-5.346	-5.252	-5.197	
$\frac{T_{yB}}{qa}$						
HDF-P4-SS1	—	0.3076	0.3154	0.3179	0.3208	0.333
S8R	0.5224	0.3975	0.3394	0.3392	0.3392	
Present	0.3415	0.3335	0.3371	0.3383	0.3387	
$\frac{T_{xD}}{qa}$						
HDF-P4-SS1	—	0.4226	0.4095	0.3875	0.3697	0.419
S8R	0.3978	0.3563	0.3708	0.3810	0.3883	
Present	0.4178	0.4157	0.4129	0.4133	0.4137	

**Table XI.**  
The dimensionless results of displacements and resultants at certain positions for the SS\*SS\* square plate

**Sources:** Kant ([Kant and Gadgil, 2002](#); [Kant and Hinton, 1983](#)); HDF-P4-FREE ([Shang et al., 2015](#)); S8R ([Abaqus, 2009](#))

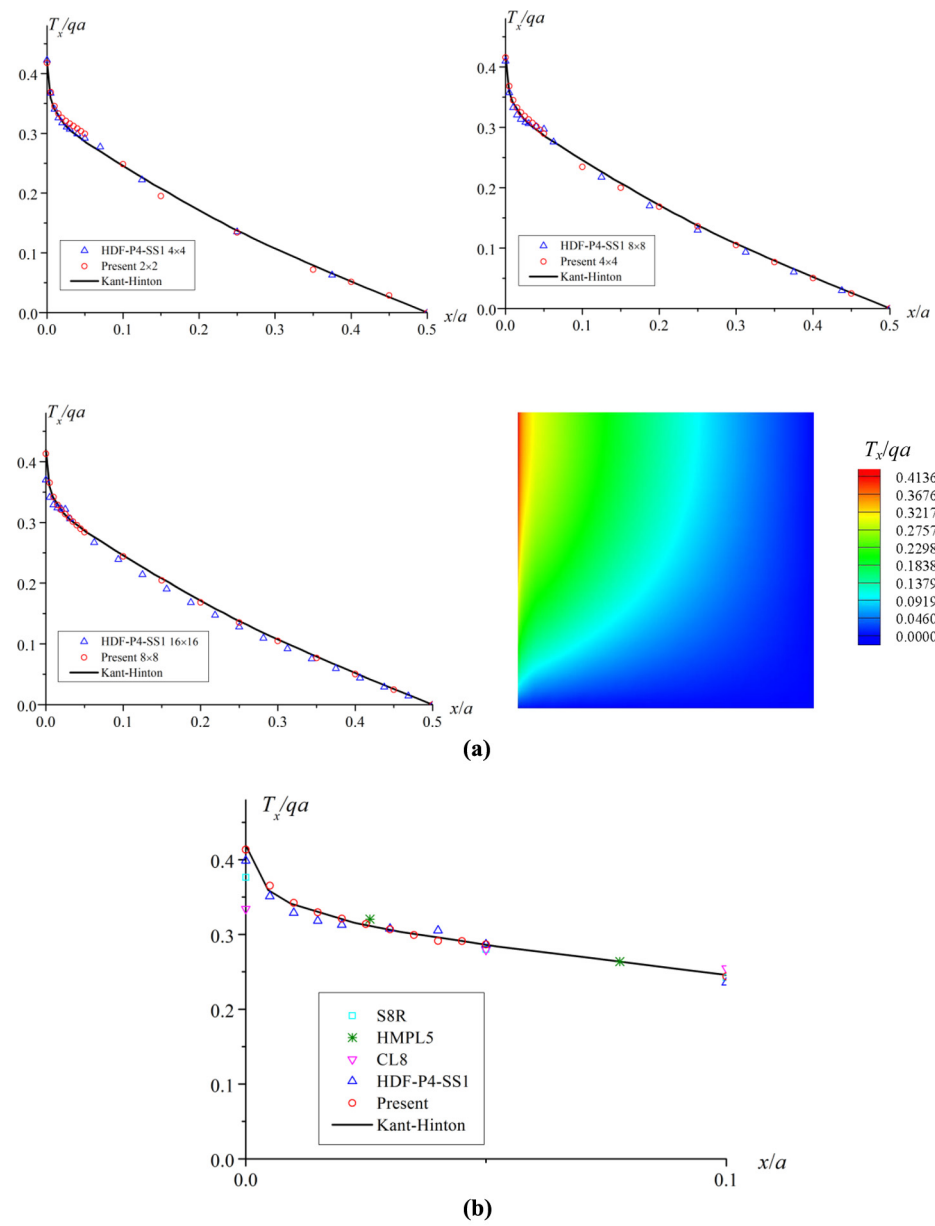
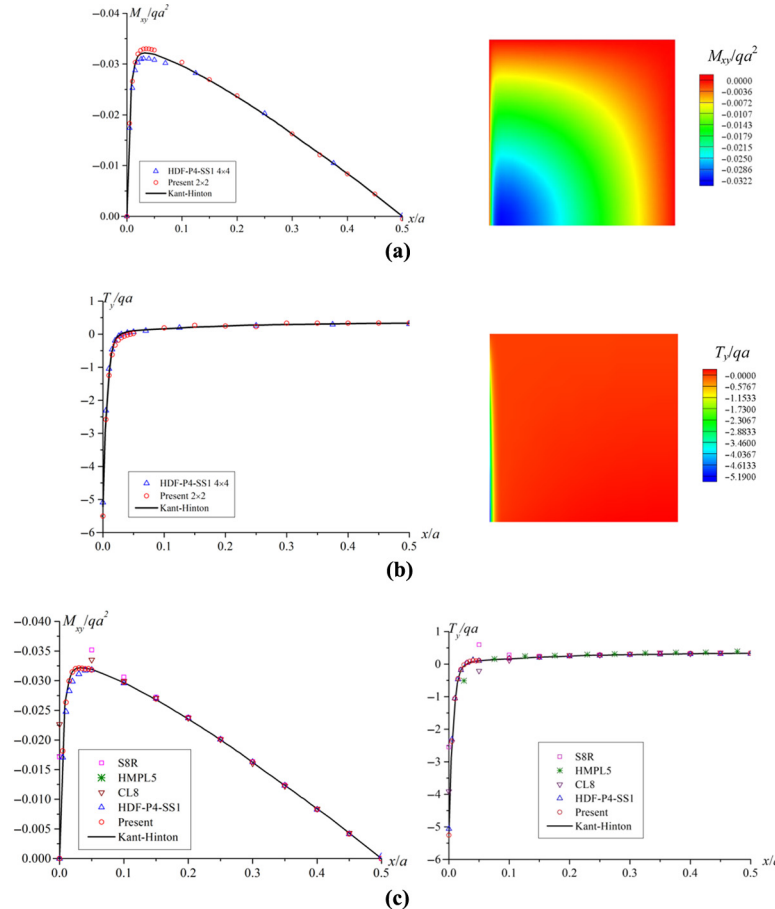


**Figure 17.**  
 Distributions,  
 contour plots and  
 comparisons of the  
 shear force  $T_x$  for the  
 SS\*SS\* case

**Notes:** (a) Distributions of the shear force  $T_x$  along the symmetric edge CD ( $y = 0.5a$ ) with i)  $2 \times 2$  mesh; ii)  $4 \times 4$  mesh; iii)  $8 \times 8$  mesh; and iv) convergent contour plot with  $8 \times 8$  mesh;  
 (b) comparisons of distributions of the shear force  $T_x$  along the symmetric edge CD ( $y = 0.5a$ ) with other methods with  $10 \times 10$  mesh



**Notes:** (a) i) Distributions of the twisting moment  $M_{xy}$  along the hard simply supported edge AB ( $y = 0$ ) with  $2 \times 2$  mesh; ii) convergent contour plot with  $8 \times 8$  mesh; (b) i) distributions of the shear force  $T_y$  along the hard simply supported edge AB ( $y = 0$ ) with  $2 \times 2$  mesh; ii) convergent contour plot with  $8 \times 8$  mesh; (c) i) comparisons of distributions of the twisting moment  $M_{xy}$ ; ii) comparisons of distributions of the shear force  $T_y$  along the hard simply supported edge AB ( $y = 0$ ) with  $10 \times 10$  mesh

**Figure 18.**  
Distributions,  
contour plots and  
comparisons of the  
twisting moment  $M_{xy}$   
and the shear force  
 $T_y$  for the SS\*SS\*  
case

$10 \times 10$  mesh are also given for comparison. Same conclusions as those in previous case can be obtained.

## 5. Conclusions

In this paper, three simple high-order hybrid displacement function elements are presented for analysis of thin and moderately thick plates. In general situation, the displacement function  $F$ , which can be used to derive displacement components satisfying all governing equations, is combined with the locking-free arbitrary-order Timoshenko's beam functions. Then, an eight-node, 24-DOF quadrilateral plate bending element, HDF-P8-23 $\beta$ , is formulated. For the special situation consisting of the edge effect or the boundary layer effect (SS1 or FREE type), an additional displacement function  $f$  related to the edge effect is considered to develop novel plate-bending elements HDF-P8-SS1 or HDF-P8-FREE.

Numerical examples show that the proposed elements are free of shear-locking, pass all patch tests, exhibit excellent convergence and possess higher precision when compared to other existing models, even when quite coarse and extremely distorted meshes are used. Especially, they can effectively solve the edge effect by accurately capturing the peak value and the sharp changes of stress/resultant-force near the SS1 or free boundary.

The proposed method possesses advantages from both analytical and discrete methods, and can be easily integrated into the standard framework of finite element programs. An interesting future work is to develop a high-performance plate crack element, and then combine the proposed elements with plate crack element to solve the plate crack propagation problem of the plate.

## References

- Abaqus (2009), *HTML Documentation*, Abaqus 6.9, Dassault Systèmes Simulia Corporation, Providence, RI.
- Ahmad, S., Irons, M. and Zienkiewicz, O.C. (1970), "Analysis of thick and thin shell structures by curved finite elements", *International Journal for Numerical Methods in Engineering*, Vol. 2, pp. 419-451.
- Arnold, D.N. and Falk, R.S. (1989), "Edge effects in the Reissner-Mindlin plate theory", *Analytical and Computational Models for Shells*, San Francisco, California, pp. 71-90.
- Arnold, D.N. and Falk, R.S. (1990), "The boundary layer for the Reissner-Mindlin plate model", *SIAM Journal on Mathematical Analysis*, Vol. 21 No. 2, pp. 281-312.
- Ayad, R., Dhatt, G. and Batoz, J.L. (1998), "A new hybrid-mixed variational approach for Reissner-Mindlin plates: the MISP model", *International Journal for Numerical Methods in Engineering*, Vol. 42, pp. 1149-1179.
- Ayad, R. and Rigolot, A. (2002), "An improved four-node hybrid-mixed element based upon Mindlin's plate theory", *International Journal for Numerical Methods in Engineering*, Vol. 55, pp. 705-731.
- Babuska, I. and Scapolla, T. (1989), "Benchmark computation and performance evaluation for a rhombic plate bending problem", *International Journal for Numerical Methods in Engineering*, Vol. 28 No. 1, pp. 155-179.
- Bathe, K.J. (1996), *Finite Element Procedures*, Prentice Hall, New Jersey, NJ.
- Bathe, K.J. and Dvorkin, E.N. (1985), "A four-node plate bending element based on Mindlin-Reissner plate theory and a mixed interpolation", *International Journal for Numerical Methods in Engineering*, Vol. 21 No. 2, pp. 367-383.
- Bathe, K.J. and Dvorkin, E.N. (1986), "A formulation of general shell elements—the use of mixed interpolation of tensorial components", *International Journal for Numerical Methods in Engineering*, Vol. 22 No. 3, pp. 697-722.

- Batoz, J.L. and Lardeur, P. (1989), "A discrete shear triangular nine DOF element for the analysis of thick to very thin plate", *International Journal for Numerical Methods in Engineering*, Vol. 28, pp. 533-560.
- Belytschko, T. and Tsay, C.S. (1983), "A stabilization procedure for the quadrilateral plate element with one point quadrature", *International Journal for Numerical Methods in Engineering*, Vol. 19 No. 3, pp. 405-419.
- Belytschko, T., Tsay, C.S. and Liu, W.K. (1981), "A stabilization matrix for the bilinear Mindlin plate element", *Computer Methods in Applied Mechanics and Engineering*, Vol. 29 No. 3, pp. 313-327.
- Briassoulis, D. (1993a), "Modeling edge effects with the C0 plate-bending elements: Part 1. analysis of the mechanism", *International Journal for Numerical Methods in Engineering*, Vol. 36 No. 23, pp. 4045-4068.
- Briassoulis, D. (1993b), "Modeling edge effects with the C0 plate-bending elements: Part 2: the performance of the reformulated four-node element", *International Journal for Numerical Methods in Engineering*, Vol. 36 No. 23, pp. 4069-4109.
- Cen, S., Fu, X.R. and Zhou, M.J. (2011a), "8- and 12-node plane hybrid stress-function elements immune to severely distorted mesh containing elements with concave shapes", *Computer Methods in Applied Mechanics and Engineering*, Vol. 200 No. 29, pp. 2321-2336.
- Cen, S., Long, Y.Q. and Yao, Z.H. (2002), "A new hybrid-enhanced displacement-based element for the analysis of laminated composite plates", *Computers & Structures*, Vol. 80 Nos 9/10, pp. 819-833.
- Cen, S., Zhou, M.J. and Fu, X.R. (2011c), "A 4-node hybrid stress-function (HS-F) plane element with drilling degrees of freedom less sensitive to severe mesh distortions", *Computers & Structures*, Vol. 89 Nos 5/6, pp. 517-528.
- Cen, S., Long, Y.Q., Yao, Z.H. and Chiew, S.P. (2006), "Application of the quadrilateral area co-ordinate method: a new element for Mindlin-Reissner plate", *International Journal for Numerical Methods in Engineering*, Vol. 66 No. 1, pp. 1-45.
- Cen, S., Shang, Y., Li, C.F. and Li, H.G. (2014), "Hybrid displacement function element method: a simple hybrid-Trefftz stress element method for analysis of Mindlin-Reissner plate", *International Journal for Numerical Methods in Engineering*, Vol. 98 No. 3, pp. 203-234.
- Cen, S. and Shang, Y. (2015), "Developments of Mindlin-Reissner plate elements", *Mathematical Problems in Engineering*, Vol. 2015, ID 456740.
- Cen, S., Fu, X.R., Zhou, G.H., Zhou, M.J. and Li, C.F. (2011b), "Shape-free finite element method: the plane hybrid stress-function (HS-F) element method for anisotropic materials", *Science China Physics, Mechanics & Astronomy*, Vol. 54 No. 4, pp. 653-665.
- Chen, W.J. and Cheung, Y.K. (2000), "Refined quadrilateral element based on Mindlin/Reissner plate theory", *International Journal for Numerical Methods in Engineering*, Vol. 47, pp. 605-627.
- Crisfield, M.A. (1984), "A quadratic Mindlin element using shear constraints", *Computers & Structures*, Vol. 18 No. 5, pp. 833-852.
- Dhananjaya, H.R., Pandey, P.C. and Nagabushanam, J. (2009), "New eight node serendipity quadrilateral plate bending element for thin and moderately thick plates using integrated force method", *Structural Engineering and Mechanics*, Vol. 33 No. 4, pp. 485-508.
- Donea, J. and Laman, L.G. (1987), "A modified representation of transverse shear in C0 quadrilateral plate elements", *Computer Methods in Applied Mechanics and Engineering*, Vol. 63, pp. 183-207.
- Falsone, G. and Settineri, D. (2012), "A Kirchhoff-like solution for the Mindlin plate model: a new finite element approach", *Mechanics Research Communications*, Vol. 40, pp. 1-10.
- Fu, X.R., Cen, S., Li, C.F. and Chen, X.M. (2010), "Analytical trial function method for development of new 8-node plane element based on the variational principle containing airy stress function", *Engineering Computations*, Vol. 27 No. 4, pp. 442-463.

- Hagglad, B. and Bathe, K.J. (1990), "Specifications of boundary-conditions for Reissner-Mindlin plate bending finite-elements", *International Journal for Numerical Methods in Engineering*, Vol. 30 No. 5, pp. 981-1011.
- Hansbo, P., Heintz, D. and Larson, M.G. (2011), "A finite element method with discontinuous rotations for the Mindlin-Reissner plate model", *Computer Methods in Applied Mechanics and Engineering*, Vol. 200 Nos 5/8, pp. 638-648.
- Hinton, E. and Huang, H.C. (1986), "A family of quadrilateral Mindlin plate element with substitute shear strain fields", *Computers & Structures*, Vol. 23 No. 3, pp. 409-431.
- Hinton, E., Selman, A. and Alkhamis, M. (1995), "Boundary-layers in uniform and variable thickness plates with rectangular and curved planforms using the finite strip method", *Communications in Numerical Methods in Engineering*, Vol. 11 No. 7, pp. 597-606.
- Hu, H.C. (1984), *Variational Principle of Theory of Elasticity with Applications*, Science press, Gordon and Breach, Science Publisher, Beijing.
- Hu, B., Wang, Z. and Xu, Y.C. (2010), "Combined hybrid method applied in the Reissner-Mindlin plate model", *Finite Elements in Analysis and Design*, Vol. 46, pp. 428-437.
- Hughes, T.J.R. and Cohen, M. (1978), "The 'heterosis' finite element for plate bending", *Computers & Structures*, Vol. 9, pp. 445-450.
- Hughes, T.J.R., Taylor, R.L. and Kanoknukulchai, W. (1977), "A simple and efficient finite element for plate bending", *International Journal for Numerical Methods in Engineering*, Vol. 11 No. 10, pp. 1529-1543.
- Ibrahimbegović, A. (1993), "Quadrilateral finite elements for analysis of thick and thin plates", *Computer Methods in Applied Mechanics and Engineering*, Vol. 110, pp. 195-209.
- Jelenic, G. and Papa, E. (2011), "Exact solution of 3D Timoshenko beam problem using linked interpolation of arbitrary order", *Archive of Applied Mechanics*, Vol. 18, pp. 171-183.
- Jin, F.S. and Qin, Q.H. (1995), "A variational principle and hybrid Trefftz finite-element for the analysis of Reissner plates", *Computers & Structures*, Vol. 56 No. 4, pp. 697-701.
- Jin, W.G., Cheung, Y.K. and Zienkiewicz, O.C. (1993), "Trefftz method for Kirchhoff plate bending problems", *International Journal for Numerical Methods in Engineering*, Vol. 36, pp. 765-781.
- Jirousek, J., Wróblewski, A. and Szybinski, B. (1995b), "A new 12 DOF quadrilateral element for analysis of thick and thin plates", *International Journal for Numerical Methods in Engineering*, Vol. 38, pp. 2619-2638.
- Jirousek, J., Wróblewski, A., Qin, Q.H. and He, X.Q. (1995a), "A family of quadrilateral hybrid-Trefftz p-elements for thick plate analysis", *Computer Methods in Applied Mechanics and Engineering*, Vol. 127, pp. 315-344.
- Kant, T. and Gadgil, M.G. (2002), "Analysis of orthotropic plates based on three theories by segmentation method", *Mechanics of Advanced Materials and Structures*, Vol. 9 No. 3, pp. 189-239.
- Kant, T. and Hinton, E. (1983), "Mindlin plate analysis by segmentation method", *Journal of Engineering Mechanics-ASCE*, Vol. 109 No. 2, pp. 537-556.
- Kant, T., Owen, D.R.J. and Zienkiewicz, O.C. (1982), "A refined higher-order C0 plate bending element", *Computers & Structures*, Vol. 15 No. 2, pp. 177-183.
- Katili, I. (1993), "A new discrete Kirchhoff-Mindlin element based on Mindlin-Reissner plate theory and assumed shear strain fields—part II: an extended DKQ element for thick-plate bending analysis", *International Journal for Numerical Methods in Engineering*, Vol. 36 No. 11, pp. 1885-1908.
- Lee, S.W. and Wong, S.C. (1982), "Mixed formulation finite elements for Mindlin theory plate bending", *International Journal for Numerical Methods in Engineering*, Vol. 18 No. 9, pp. 1297-1311.

- Li, T., Qi, Z.H., Ma, X. and Chen, W.J. (2015), "High-order assumed stress quadrilateral element for the Mindlin plate bending problem", *Structural Engineering and Mechanics*, Vol. 54 No. 3, pp. 393-417.
- Long, Y.Q., Cen, S. and Long, Z.F. (2009), *Advanced Finite Element Method in Structural Engineering*, Springer, Heidelberg & Tsinghua University Press, Beijing.
- Long, Y.Q., Li, J.X., Long, Z.F. and Cen, S. (1999a), "Area coordinates used in quadrilateral elements", *Communications in Numerical Methods in Engineering*, Vol. 15 No. 8, pp. 533-545.
- Long, Z.F., Li, J.X., Cen, S. and Long, Y.Q. (1999b), "Some basic formulae for area coordinates used in quadrilateral elements", *Communications in Numerical Methods in Engineering*, Vol. 15 No. 12, pp. 841-852.
- Mindlin, R.D. (1951), "Influence of rotatory inertia and shear on flexural motions of isotropic elastic plates", *Journal of Applied Mechanics-Transactions of the ASME*, Vol. 18 No. 1, pp. 31-38.
- Morley, L.S.D. (1963), "Skew plates and structures", *International Series of Monographs in Aeronautics and Astronautics*, Macmillan, New York, NY.
- Nguyen-Thanh, N., Rabczuk, T., Nguyen-Xuan, H. and Bordas, S. (2011), "An alternative alpha finite element method with discrete shear gap technique for analysis of isotropic Mindlin-Reissner plates", *Finite Elements in Analysis and Design*, Vol. 47 No. 5, pp. 519-535.
- Nguyen-Thoi, T., Phung-Van, P., Nguyen-Xuan, H. and Thai-Hoang, C. (2012), "A cell-based smoothed discrete shear gap method using triangular elements for static and free vibration analyses of Reissner-Mindlin plates", *International Journal for Numerical Methods in Engineering*, Vol. 91 No. 7, pp. 705-741.
- Nguyen-Xuan, H., Liu, G.R., Thai-Hoang, C. and Nguyen-Thoi, T. (2009), "An edge-based smoothed finite element method with stabilized discrete shear gap technique for analysis of Reissner-Mindlin plates", *Computer Methods in Applied Mechanics and Engineering*, Vol. 199, pp. 471-489.
- Nguyen-Xuan, H., Rabczuk, T., Bordas, S. and Debongnie, J.F. (2008), "A smoothed finite element method for plate analysis", *Computer Methods in Applied Mechanics and Engineering*, Vol. 197 Nos 13/16, pp. 1184-1203.
- Onate, E., Zienkiewicz, O.C., Suarez, B. and Taylor, R.L. (1992), "A general methodology for deriving shear constrained Reissner-Mindlin plate elements", *International Journal for Numerical Methods in Engineering*, Vol. 33 No. 2, pp. 345-367.
- Petrolito, J. (1990), "Hybrid-Trefftz quadrilateral elements for thick plate analysis", *Computer Methods in Applied Mechanics and Engineering*, Vol. 78 No. 3, pp. 331-351.
- Petrolito, J. (1996), "Triangular thick plate elements based on a hybrid-Trefftz approach", *Computers & Structures*, Vol. 60 No. 6, pp. 883-894.
- Polit, O., Touratier, M. and Lory, P. (1994), "A new eight-node quadrilateral shear-bending plate finite element", *International Journal for Numerical Methods in Engineering*, Vol. 37, pp. 387-411.
- Rao, N.V.R., Ozakca, M. and Hinton, E. (1992), "A study of boundary-layers in plates using Mindlin-Reissner and 3-D elements", *International Journal for Numerical Methods in Engineering*, Vol. 33 No. 6, pp. 1305-1320.
- Reissner, E. (1945), "The effect of transverse shear deformation on the bending of elastic plates", *Journal of Applied Mechanics-Transactions of the ASME*, Vol. 12 No. 2, pp. 69-77.
- Rezaiee-Pajand, M. and Karkon, M. (2012), "Two efficient hybrid-Trefftz elements for plate bending analysis", *Latin American Journal of Solids and Structures*, Vol. 9 No. 1, pp. 43-67.
- Ribaric, D. and Jelenic, G. (2012), "Higher-order linked interpolation in quadrilateral thick plate finite elements", *Finite Elements in Analysis and Design*, Vol. 51, pp. 67-80.
- Saleeb, A.F. and Chang, T.Y. (1987), "An efficient quadrilateral element for plate bending analysis", *International Journal for Numerical Methods in Engineering*, Vol. 24 No. 6, pp. 1123-1155.

- 
- Schwab, C. and Suri, M. (1996), "The p and HP versions of the finite element method for problems with boundary layers", *Mathematics of Computation*, Vol. 65 No. 216, pp. 1403-1429.
- Shang, Y., Cen, S., Li, C.F. and Huang, J.B. (2015), "An effective hybrid displacement function element method for solving the edge effect of Mindlin-Reissner plate", *International Journal for Numerical Methods in Engineering*, Vol. 102, pp. 1449-1487.
- Soh, A.K., Long, Z.F. and Cen, S. (1999a), "A Mindlin plate triangular element with improved interpolation based on Timoshenko's beam theory", *Communications in Numerical Methods in Engineering*, Vol. 15 No. 7, pp. 527-532.
- Soh, A.K., Long, Z.F. and Cen, S. (1999b), "A new nine DOF triangular element for analysis of thick and thin plates", *Computational Mechanics*, Vol. 24 No. 5, pp. 408-417.
- Soh, A.K., Cen, S., Long, Y.Q. and Long, Z.F. (2001), "A new twelve DOF quadrilateral element for analysis of thick and thin plates", *European Journal of Mechanics A-Solids*, Vol. 20 No. 2, pp. 299-326.
- Spilker, R.L. (1982), "Invariant 8-node hybrid stress element for thin and moderately thick plates", *International Journal for Numerical Methods in Engineering*, Vol. 18, pp. 1153-1178.
- Spilker, R.L. and Munir, N.I. (1980), "A serendipity cubic-displacement hybrid-stress for thin and moderately thick plate", *International Journal for Numerical Methods in Engineering*, Vol. 15, pp. 1261-1278.
- Taylor, R.L. and Auricchio, F. (1993), "Linked interpolation for Reissner-Mindlin plate elements: Part II—a simple triangle", *International Journal for Numerical Methods in Engineering*, Vol. 36 No. 18, pp. 3057-3066.
- Wang, C.M., Wang, Y.C., Reddy, J.N. and Thevendran, V. (2002), "Improved computation of stress resultants in the p-Ritz method", *Journal of Engineering Mechanics-ASCE*, Vol. 128 No. 2, pp. 249-257.
- Ye, K.S. and Yuan, S. (2002), "Analysis of shells by finite element method of lines (II): numerical examples", *Engineering Mechanics*, Vol. 19 No. 5, pp. 16-23. (in Chinese).
- Yuan, S. (1993), *The Finite Element Method of Lines: Theory and Applications*, Science Press, Beijing & New York.
- Yuan, S., Jin, Y. and Williams, F.W. (1998), "Bending analysis of Mindlin plates by extended Kantorovich method", *Journal of Engineering Mechanics-ASCE*, Vol. 124 No. 12, pp. 1339-1345.
- Zhang, H.X. and Kuang, J.S. (2007), "Eight-node reissner-mindlin plate element based on boundary interpolation using Timoshenko beam function", *International Journal for Numerical Methods in Engineering*, Vol. 69, pp. 1345-1373.
- Zienkiewicz, O.C. and Taylor, R.L. (2000), *The Finite Element Method, Solid Mechanics*, 5th ed., Butterworth-Heinemann, Oxford, Vol. 2.
- Zienkiewicz, O.C., Taylor, R.L. and Too, J.M. (1971), "Reduced integration technique in general analysis of plates and shells", *International Journal for Numerical Methods in Engineering*, Vol. 38 No. 2, pp. 275-290.
- Zienkiewicz, O.C., Xu, Z.N., Zeng, L.F. and Samuelsson, A. (1993), "Linked interpolation for Reissner-Mindlin plate element: part I—a simple quadrilateral", *International Journal for Numerical Methods in Engineering*, Vol. 36 No. 18, pp. 3043-3056.

**Corresponding author**

Song Cen can be contacted at: [censong@mail.tsinghua.edu.cn](mailto:censong@mail.tsinghua.edu.cn)

---

## Appendix

Eight-node  
elements

### The expressions for matrix $\bar{\mathbf{N}}|_{\Gamma}$ in equation (12)

The  $i-j-k$  boundary displacement vector of the element  $\bar{\mathbf{N}}|_{\Gamma}$  can be rewritten as:

$$\bar{\mathbf{d}} = \begin{Bmatrix} \bar{\psi}_n \\ \bar{\psi}_s \\ \bar{w} \end{Bmatrix} = \mathbf{L}_d \bar{\mathbf{u}}_{ijk} = \bar{\mathbf{N}}|_{\Gamma} \mathbf{q}^e \quad \text{585}$$


---

(A1)

In which the vector  $\bar{\mathbf{u}}_{ijk}$  is given by [equation \(6\)](#); and  $\mathbf{L}_d$  is the direction matrix:

$$\mathbf{L}_d = \begin{bmatrix} 0 & l_x & l_y \\ 0 & -l_y & l_x \\ 1 & 0 & 0 \end{bmatrix} \quad \text{(A2)}$$

- Along 1-2-5 boundary:

$$\bar{\mathbf{N}}|_{\Gamma} = [\mathbf{N}_1 \quad \mathbf{N}_2 \quad \mathbf{0} \quad \mathbf{0} \quad \mathbf{N}_5 \quad \mathbf{0} \quad \mathbf{0} \quad \mathbf{0}] \quad \text{(A3)}$$

where:

$$\mathbf{N}_1 = \begin{bmatrix} 0 & I_a l_x & I_a l_y \\ 0 & -I_a l_y & I_a l_x \\ I_a & -I_0 l_x^* & I_0 l_y^* \end{bmatrix}, \mathbf{N}_2 = \begin{bmatrix} 0 & I_b l_x & I_b l_y \\ 0 & -I_b l_y & I_b l_x \\ I_b & -I_0 l_x^* & I_0 l_y^* \end{bmatrix}, \mathbf{N}_5 = \begin{bmatrix} 0 & I_c l_x & I_c l_y \\ 0 & -I_c l_y & I_c l_x \\ I_c & 2I_0 l_x^* & -2I_0 l_y^* \end{bmatrix} \quad \text{(A4)}$$

And  $\mathbf{0}$  is a  $3 \times 3$  zero matrix.

- Along 2-3-6 boundary:

$$\bar{\mathbf{N}}|_{\Gamma} = [\mathbf{0} \quad \mathbf{N}_2 \quad \mathbf{N}_3 \quad \mathbf{0} \quad \mathbf{0} \quad \mathbf{N}_6 \quad \mathbf{0} \quad \mathbf{0}] \quad \text{(A5)}$$

where:

$$\mathbf{N}_2 = \begin{bmatrix} 0 & I_a l_x & I_a l_y \\ 0 & -I_a l_y & I_a l_x \\ I_a & -I_0 l_x^* & I_0 l_y^* \end{bmatrix}, \mathbf{N}_3 = \begin{bmatrix} 0 & I_b l_x & I_b l_y \\ 0 & -I_b l_y & I_b l_x \\ I_b & -I_0 l_x^* & I_0 l_y^* \end{bmatrix}, \mathbf{N}_6 = \begin{bmatrix} 0 & I_c l_x & I_c l_y \\ 0 & -I_c l_y & I_c l_x \\ I_c & 2I_0 l_x^* & -2I_0 l_y^* \end{bmatrix} \quad \text{(A6)}$$

- Along 3-4-7 boundary:

$$\bar{\mathbf{N}}|_{\Gamma} = [\mathbf{0} \quad \mathbf{0} \quad \mathbf{N}_3 \quad \mathbf{N}_4 \quad \mathbf{0} \quad \mathbf{0} \quad \mathbf{N}_7 \quad \mathbf{0}] \quad \text{(A7)}$$

where:

$$\mathbf{N}_3 = \begin{bmatrix} 0 & I_a l_x & I_a l_y \\ 0 & -I_a l_y & I_a l_x \\ I_a & -I_0 l_x^* & I_0 l_y^* \end{bmatrix}, \mathbf{N}_4 = \begin{bmatrix} 0 & I_b l_x & I_b l_y \\ 0 & -I_b l_y & I_b l_x \\ I_b & -I_0 l_x^* & I_0 l_y^* \end{bmatrix}, \mathbf{N}_7 = \begin{bmatrix} 0 & I_c l_x & I_c l_y \\ 0 & -I_c l_y & I_c l_x \\ I_c & 2I_0 l_x^* & -2I_0 l_y^* \end{bmatrix} \quad (\text{A8})$$

- Along 4-1-8 boundary:

$$\bar{\mathbf{N}}|_{\Gamma} = [\mathbf{N}_1 \quad \mathbf{0} \quad \mathbf{0} \quad \mathbf{N}_4 \quad \mathbf{0} \quad \mathbf{0} \quad \mathbf{0} \quad \mathbf{N}_8] \quad (\text{A9})$$

where:

$$\mathbf{N}_4 = \begin{bmatrix} 0 & I_a l_x & I_a l_y \\ 0 & -I_a l_y & I_a l_x \\ I_a & -I_0 l_x^* & I_0 l_y^* \end{bmatrix}, \mathbf{N}_1 = \begin{bmatrix} 0 & I_b l_x & I_b l_y \\ 0 & -I_b l_y & I_b l_x \\ I_b & -I_0 l_x^* & I_0 l_y^* \end{bmatrix}, \mathbf{N}_8 = \begin{bmatrix} 0 & I_c l_x & I_c l_y \\ 0 & -I_c l_y & I_c l_x \\ I_c & 2I_0 l_x^* & -2I_0 l_y^* \end{bmatrix} \quad (\text{A10})$$

The relevant parameters and matrices have been given in equations (3) to (7).